

การจำลองอันตรกิริยาของแอนติโปรตอน-โปรตอน โดยใช้แบบจำลอง
พลศาสตร์ควอนตัมเชิงโมเลกุลเหนือสัมพัทธภาพ

นายอายุท ลิมพิรัตน์

วิทยานิพนธ์นี้เป็นส่วนหนึ่งของการศึกษาตามหลักสูตรปริญญาวิทยาศาสตรมหาบัณฑิต
สาขาวิชาฟิสิกส์
มหาวิทยาลัยเทคโนโลยีสุรนารี
ปีการศึกษา 2547
ISBN 974-533-438-3

**SIMULATION OF ANTIPROTON-PROTON
INTERACTIONS USING
ULTRARELATIVISTIC QUANTUM
MOLECULAR DYNAMICS MODEL**

Mr. Ayut Limphirat

A Thesis Submitted in Partial Fulfillment of the Requirements for the

Degree of Master of Science in Physics

Suranaree University of Technology

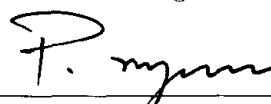
Academic Year 2004

ISBN 974-533-438-3

**SIMULATION OF ANTIPROTON-PROTON
INTERACTIONS USING ULTRARELATIVISTIC
QUANTUM MOLECULAR DYNAMICS MODEL**

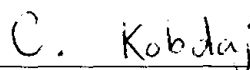
Suranaree University of Technology has approved this thesis submitted in partial fulfillment of the requirements for a Master's Degree.

Thesis Examining Committee



(Asst. Prof. Dr. Prapun Manyum)

Chairperson



(Dr. Chinorat Kobdaj)

Member (Thesis Advisor)



(Assoc. Prof. Dr. Yupeng Yan)

Member



(Assoc. Prof. Dr. Prasart Suebka)

Member

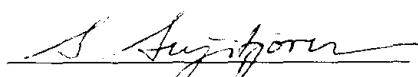


(Col. Dr. Worasit Uchai)

Member



(Assoc. Prof. Dr. Prasart Suebka)



(Assoc. Prof. Dr. Sarawut Sujitjorn)

Vice Rector for Academic Affairs

Dean of Institute of Science

อายุทธ ลิมพิรัตน์ : การจำลองอันตรกิริยาของแอนติโปรตอน-โปรตอน โดยใช้
แบบจำลองพลศาสตร์ควอนตัมเชิงโมเลกุลเหนือสัมพัทธภาพ (SIMULATION OF
ANTIPROTON-PROTON INTERACTIONS USING ULTRARELATIVIS-
TIC QUANTUM MOLECULAR DYNAMICS MODEL) อาจารย์ที่ปรึกษา :
ดร.ชินรัตน์ กอบเดช, 54 หน้า. ISBN 974-533-438-3

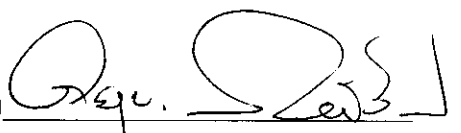
แบบจำลองพลศาสตร์ควอนตัมเชิงโมเลกุลเหนือสัมพัทธภาพถูกนำมาใช้เพื่อศึกษาอันตรกิริยาของแอนติโปรตอน-โปรตอน ที่พลังงานศูนย์กลางมวล 20 40 80 และ 160 จิกะอิเล็กตรอนโวลต์ จากการศึกษาพบว่า จำนวนอนุภาครวมทั้งหมดที่เกิดขึ้นเพิ่มขึ้นเล็กน้อยเมื่อพลังงานศูนย์กลางมวลเพิ่มขึ้นในช่วง 20 ถึง 160 จิกะอิเล็กตรอนโวลต์ อนุภาคแต่ละชนิดมีจำนวนใกล้เคียงกันที่พลังงานต่างกัน โดยจำนวนอนุภาคพายออนมีมากกว่าโปรตอน แอนติโปรตอนและนิวตรอน จำนวนอนุภาคเกาออนมีน้อยสุด การแจกแจงแบบรวดเร็วของอนุภาคสุดท้ายจากอันตรกิริยา แสดงให้เห็นว่า เกิดอนุภาคประจุบวกส่วนใหญ่ในทิศทางเดียวกับโปรตอน เกิดอนุภาคประจุลบส่วนใหญ่ในทิศทางเดียวกับแอนติโปรตอน และเกิดอนุภาคพลังงานสูงมากขึ้นเมื่อพลังงานศูนย์กลางมวลมีค่าสูงขึ้น

สาขาวิชาฟิสิกส์
ปีการศึกษา 2547

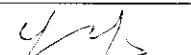
ลายมือชื่อนักศึกษา

ลายมือชื่ออาจารย์ที่ปรึกษา

ลายมือชื่ออาจารย์ที่ปรึกษาร่วม



ชินรัตน์ กอบเดช



AYUT LIMPHIRAT : SIMULATION OF ANTIPROTON- PROTON
INTERACTIONS USING ULTRARELATIVISTIC QUANTUM
MOLECULAR DYNAMICS MODEL. THESIS ADVISOR : CHINORAT
KOBDAJ, Ph.D. 54 PP. ISBN 974-533-438-3

ANTIPROTON-PROTON/UrQMD/RAPIDITY/TRANSVERSE MASS

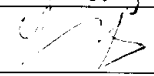
The $\bar{p}p$ collision is preliminarily studied using the Ultrarelativistic Quantum Molecular Dynamics model (UrQMD) at energies $\sqrt{s} = 20, 40, 80$ and 160 GeV. It is found that the total yield for all particles increases slightly with the center-of-mass energies ranging from 20 to 160 GeV, the yields for a certain particle at different energies are almost the same, the yields of pions in the reaction are higher than those for p , \bar{p} and n , and the productions of kaons are very low. The rapidity distribution of final particles indicates that more positively-charged particles are produced in the p direction while more negatively-charged particles are produced in the \bar{p} direction, and more particles with higher energies are produced with increasing the energy \sqrt{s} .

School of Physics

Academic Year 2004

Student's Signature Ayut Liphirat

Advisor's Signature C. Kobdaj

Co-advisor's Signature 

ACKNOWLEDGEMENTS

I am grateful to my thesis supervisors, Dr. Chinorat Kobdaj and Assoc. Prof. Dr. Yupeng Yan for their guidance throughout this work. They set up the research project and gave me a very good research experience. I have learnt not only the relevant physics but also the spiritual attitude.

I would like to thank Prof. Dr. Horst Stoecker and Prof. Dr. Marcus Bleicher for their guidance during my research at the Institute for Theoretical Physics, Frankfurt University, Germany.

I would like to thank Assoc. Prof. Dr. Prasart Suebka, Col. Dr. Worasit Uchai and Asst. Prof. Dr. Prapun Manyum for their kindness and being Thesis Examining Committee.

I wish to thank Dr. Khanchai Kosonthongkee and Miss Pornrad Srisawad for their cooperation on this work. Thanks to Dr. Jessada Tanthanuch for his consistent help, especially in building up the SUT-thesis format in Latex.

I acknowledge the financial support in part for 2 years by the National Research Council of Thailand (NRCT) under Grant No. 1.CH7/2545 and 1.CH28/2546.

I would like to thank my grandparents and my parents for their understanding, support and encouragement over the years of my study.

I would like to thank all my friends for all good things they gave to me.

Finally, It is a pleasure for me to thank again Dr. Chinorat Kobdaj and Dr. Yupeng Yan for their kindness and financial support during my study at SUT.

Ayut Limphirat

CONTENTS

	Page
ABSTRACT IN THAI	I
ABSTRACT IN ENGLISH	II
ACKNOWLEDGEMENTS	III
CONTENTS	IV
LIST OF TABLES	VI
LIST OF FIGURES	VII
 CHAPTER	
I INTRODUCTION	1
II THE UrQMD MODEL	6
2.1 Initialization	7
2.2 Equations of motion	8
2.3 The collision term	12
III NUMERICAL CALCULATIONS	18
3.1 $Pb + Pb$ Interactions	19
3.2 $p + p$ Interactions	23

CONTENTS (Continued)

	Page
IV RESULTS AND DISCUSSIONS	28
4.1 Particle Yields	28
4.2 Rapidity distribution	32
4.3 Transverse mass distribution	42
4.4 Summary	48
REFERENCES	50
CURRICULUM VITAE	54

LIST OF TABLES

Table	Page
2.1 Parameters of the hard equation of state implemented in the UrQMD model, with and without Pauli-potential.	12
2.2 Baryons and baryon-resonances included into the UrQMD model. Through baryon-antibaryon symmetry the respective antibaryon states are included as well.	14
2.3 Mesons and meson-resonances, sorted with respect to spin and parity, included into the UrQMD model.	15
2.4 Parameters for the CERN/HERA parameterization for the total and elastic antiproton -proton cross-sections. This parameterization is used in UrQMD for momenta $p_{lab} > 5\text{GeV}/c$	16
3.1 Fitted parameters of the 2-G parametrization of rapidity distributions measured for π^- , K^+ , K^- mesons produced in central $Pb + Pb$ collisions at 40, 80 and 160 AGeV.	22
4.1 Particle yields per event.	29
4.2 Ratios of yields for individual particles.	30

LIST OF FIGURES

Figure	Page
2.1 The $\bar{p}p$ cross-section as compared to the experimental data (Barnett et al., 1996) on total (open circles), elastic (open squares), and annihilation (open triangles) cross-sections. The diffractive cross-section is assumed to be a difference between the total cross-section and the sum of the elastic and annihilation cross-section.	15
3.1 The NA49 experimental setup. (Available: http://na49info.cern.ch/) . . .	20
3.2 Rapidity distributions of π^- , K^+ and K^- mesons produced in central $Pb + Pb$ collisions at 40, 80 and 160 AGeV. The closed symbols indicate measured points, open points are reflected with respect to midrapidity. The lines indicate 2-G fits to spectra [see Eq.(3.2)].	21
3.3 The rapidity distribution of π^- , K^+ and K^- in 7% or 5% central $Pb + Pb$ collisions at 40, 80 and 160 AGeV calculated within the UrQMD model (solid lines) version 1.3 in comparison with the experimental data from the NA49 Collaboration at 40, 80 and 160 AGeV (the symbol represent π^- , K^+ and K^- experimental data).	24
3.4 The transverse mass spectra at midrapidity for π^- , K^+ and $K^- (\times 0.1)$ (long dashed line, dot line and dashed line respectively) from $p + p$ reactions at 160 GeV from UrQMD version 1.3. The thin lines correspond to fits of experimental slope parameters from NA49 (Kraus, 2004).	26

LIST OF FIGURES (Continued)

Figure	Page
3.5 The transverse mass spectra at midrapidity for π^- and K^- from $p + p$ reactions at $\sqrt{s} = 200$ GeV from UrQMD version 1.3 (dot and dashed lines, multiplied by a factor of 2). The square and dot symbols indicate the data from the STAR Collaboration (Barannikova and Wang, 2003).	27
4.1 Particle yields ratios for nucleon, antinucleon, pions and kaons.	31
4.2 The rapidity distribution of p in $\bar{p} + p$ collisions at $\sqrt{s} = 20, 40, 80$ and 160 GeV calculated within the UrQMD model.	33
4.3 The rapidity distribution of \bar{p} in $\bar{p} + p$ collisions at $\sqrt{s} = 20, 40, 80$ and 160 GeV calculated within the UrQMD model.	34
4.4 The rapidity distribution of π^0 in $\bar{p} + p$ collisions at $\sqrt{s} = 20, 40, 80$ and 160 GeV calculated within the UrQMD model.	35
4.5 The rapidity distribution of π^+ in $\bar{p} + p$ collisions at $\sqrt{s} = 20, 40, 80$ and 160 GeV calculated within the UrQMD model.	36
4.6 The rapidity distribution of π^- in $\bar{p} + p$ collisions at $\sqrt{s} = 20, 40, 80$ and 160 GeV calculated within the UrQMD model.	37
4.7 The rapidity distribution of n in $\bar{p} + p$ collisions at $\sqrt{s} = 20, 40, 80$ and 160 GeV calculated within the UrQMD model.	38
4.8 The rapidity distribution of \bar{n} in $\bar{p} + p$ collisions at $\sqrt{s} = 20, 40, 80$ and 160 GeV calculated within the UrQMD model.	39
4.9 The rapidity distribution of K^+ in $\bar{p} + p$ collisions at $\sqrt{s} = 20, 40, 80$ and 160 GeV calculated within the UrQMD model.	40

LIST OF FIGURES (Continued)

Figure	Page
4.10 The rapidity distribution of K^- in $\bar{p} + p$ collisions at $\sqrt{s} = 20, 40, 80$ and 160 GeV calculated within the UrQMD model.	41
4.11 The rapidity distribution of K^0 in $\bar{p} + p$ collisions at $\sqrt{s} = 20, 40, 80$ and 160 GeV calculated within the UrQMD model.	43
4.12 The rapidity distribution of \bar{K}^0 in $\bar{p} + p$ collisions at $\sqrt{s} = 20, 40, 80$ and 160 GeV calculated within the UrQMD model.	44
4.13 Transverse mass distribution of p, \bar{p}, n, \bar{n} in $\bar{p} + p$ collisions at $\sqrt{s} = 20, 40, 80$ and 160 GeV calculated within the UrQMD model.	45
4.14 Transverse mass distribution of π^0, π^+, π^- in $\bar{p} + p$ collisions at $\sqrt{s} = 20, 40, 80$ and 160 GeV calculated within the UrQMD model.	46
4.15 Transverse mass distribution of K^+, K^-, K^0, \bar{K}^0 in $\bar{p} + p$ collisions at $\sqrt{s} = 20, 40, 80$ and 160 GeV calculated within the UrQMD model.	47

CHAPTER I

INTRODUCTION

Proton is a subatomic particle with a positively fundamental electric charge of 1.6×10^{-19} C and mass of 938.280 MeV ($1.6726231 \times 10^{-27}$ kg). It is consisted of two up quarks and one down quark (uud) and classified as baryons. In nature, the proton is observed to be stable because its half life is greater than 10^{32} years.

The antiparticle of a proton is called antiproton. It has the same mass as proton with a negative charge. Antiproton is consisted of two anti-up quarks and one anti-down quark ($\bar{u}\bar{u}\bar{d}$).

The study of antiproton-proton collisions may be grouped into low and high energy regimes, that is, non-relativistic collisions at the low-energy antiproton ring (LEAR) and relativistic collisions at Super Proton Synchrotron (SPS).

Experiments with low-energy antiprotons, particular at LEAR in European Organization for Nuclear Research (CERN), have produced a wealth of information on the dynamics of the strongly interacting nucleon-antinucleon ($N\bar{N}$) system. The $N\bar{N}$ interactions is a subject to the experimental and the theoretical investigations more than 30 years. Thereby, the $N\bar{N}$ annihilation, due to its richness of possible final meson states, is considered to be a fertile testing ground for the non-perturbative regime of quantum chromodynamics (QCD) (Muhm, Gutsche, Thierauf, Yan and Faessler, 1996).

The study of antiproton-proton collision at relativistic energy became available when Simon van der Meer at European Organization for Nuclear Research (CERN) invented a technique that now made it possible to accumulate, concen-

trate and control antiproton beam (Mohl, Petrucci, Thorndahl and van der Meer, 1980) in the early 1980s. The accelerator that is used to study proton-antiproton collisions at CERN is called Super Proton Synchrotron (SPS). At that time, it had the energy of 300 GeV. In 1983, the UA1 experimental team, led by Carlo Rubbia, saw two new particles, the W boson and Z boson, being produced in proton antiproton collisions (Arnison et al., 1983). Today the most powerful proton-antiproton collider is Tevatron at Fermilab, Chicago, with a collision energy up to 1.8 TeV. In 1995, the study of proton antiproton collision ($p\bar{p}$) gave the evidence of the top quark (Abachi et al., 1995; Abachi, Abbott et al., 1995). In the same year, D0 Collaboration at Fermilab reported a measurement of the inclusive muon and b-quark production cross section in $p\bar{p}$ collisions at center of mass energy $\sqrt{s} = 1.8$ TeV (Abachi, Abbott, Abolins et al., 1995). Later, in 1996 D0 Collaboration measured the production cross-section of single, isolated photon which transverse energies is in the range of 10-125 GeV in $p\bar{p}$ collisions at $\sqrt{s} = 1.8$ TeV (Abachi, Abbott, Abolins, Acharya et al., 1996). In 1998, the Collide Detector at Fermilab Collaboration presented a measurement of the differential cross section for the production of multijet events in $p\bar{p}$ collisions (Abe et al., 1998).

As mention above, the study of $p\bar{p}$ collision has given a number of important results in elementary particle physics. To understand each process, we use theoretical models to explain the collision. There are a number of models except Ultrarelativistic Quantum Molecular Dynamics model (UrQMD) (Bass, Belkacem, Bleicher et al., 1998). Here, we would like to give a short review of some important models such as Boltzmann Uehling Uhlenbeck model (BUU), Vlasov Uehling Uhlenbeck model (VUU) (Aichelin, Peilert, Bohnet, Rosenhauer, Stoecker and Griner, 1998; Kruse, Jacak, Molitoris, Westfall and Stoecker, 1985) and others.

E.A. Uhling and G.E. Uhlenbeck studied nuclear collisions using Uhling Uhlenbeck equation (Uhling and Uhlenbeck, 1933). Later, BUU model (Aichelin, Peilert, Bohnet, Rosenhauer, Stoecker and Griner, 1998) was used to study heavy ion collisions with the incident particle energies over 25 MeV/nucleon and the production of medium mass clusters with atomic number between 5 and 30. But the results in BUU model do not fit with the data because it used only classical potentials.

The VUU model (Kruse, Jacak, Molitoris, Westfall and Stoecker, 1985) was developed for the same objective as the BUU model with the attempt to treat interactions in the form of mean field potentials and to describe each particle after collisions. However, the mean field potential is not completed since it is not cover the effect of many body collisions. Therefore, the results from VUU model can not match the experimental data.

Another approach to study the collision is the microscopic model such as Time Dependent Hartree-Fock (TDHF) (Bonche, Koonin and Negele, 1976), Classical Molecular Dynamics model (CMD) (Bodmer and Panos, 1977) and Quantum Molecular Dynamics model (QMD) (Aichelin, 1991). Time Dependent Hartree-Fock (Bonche, Koonin and Negele, 1976) was suggested by Dirac to explain the collisions in term of parameter density and temperature.

Classical Molecular Dynamics model (CMD) (Bodmer and Panos, 1977) is a microscopic model which can be used to find out heavy-ion collision cross sections. To obtain the cross-section in the CMD model, it is necessary to know nucleon-nucleon interactions and other values such as momenta which can be calculated from equation of motion of incident nucleons. However, the CMD can not give a good prediction when the energy of particles is greater than 100 MeV. To improve the CMD model one moves onto quantum mechanics by representing each nucleon

by a Gaussian wave function and considering the interaction among only two and three particles. This new model is called Quantum Molecular Dynamics model (QMD) (Aichelin, 1991). The validity of this model is in the intermediate energy region, that is, from 100 MeV to 2 GeV.

If the energy is higher than 2 GeV, the relativistic effect has to be included into the model. The model has now become the so-called Ultrarelativistic Quantum Molecular Dynamics model (UrQMD) (Bass, Belkacem, Bleicher et al., 1998; Bleicher et al., 1999).

In the experimental sector, the heavy ion facilities have been working mainly in three energy regimes: i) energy about 1 AGeV at BEVALAC in Berkeley, USA or SchwerIonenSynchrotron (SIS) at GSI-Darmstadt, Germany; ii) energy about 2-15 AGeV at the Alternating Gradient Synchrotron (AGS), in Brookhaven; iii) at the Super Proton Synchrotron (SPS) in CERN, energy about 40-200 AGeV. In the future, much higher energies will be available at the Relativistic Heavy Ion Collider (RHIC) in Brookhaven ($\sqrt{s} \approx 200$ AGeV) and the Large Hardron Collider (LHC) in CERN ($\sqrt{s} \approx 6$ ATeV).

The aim of this project is (1) to understand the UrQMD code by calculating the particle rapidity and transverse mass distributions for nucleus-nucleus collisions and comparing our results with published results from other groups, and (2) to preliminarily study the antiproton-proton collisions at center of mass energies from 20 to 160 GeV using UrQMD model. The particle yield and the rapidity and transverse mass distributions of the particles $p, \bar{p}, n, \bar{n}, \pi^+, \pi^-, \pi^0, K^+, K^-, K^0$ and \bar{K}^0 are considered.

The work is structured as follows: A brief description of the UrQMD model, which is used in the work, is given in Chapter II. The first part of Chapter III shows the repeated results for $Pb + Pb$ collisions while the second part of Chapter

III shows the repeated result for $p + p$ collisions. The last chapter (Chapter IV) gives our all results and conclusions.

CHAPTER II

THE UrQMD MODEL

The Ultrarelativistic Quantum Molecular Dynamics (UrQMD) model has been developed over ten years by hundreds of physicists since it was initiated by Frankfurt Heavy-Ion Group, Institute for Theoretical Physics, Frankfurt University. The main goals are to gain understandings, within a single transport model, of the following physical phenomena such as: creation of dense hadronic matter at high temperatures; properties of nuclear matter, delta and resonance matter; creation of mesonic matter and of anti-matter; creation and transport of rare particles in hadronic matter; creation, modification and destruction of strangeness in matter; emission of electromagnetic probes. The model describe the relativistic heavy ion collisions in the energy range from AGS (Alternating Gradient Synchrotron, Brookhaven) up to SPS (Super Proton Synchrotron, CERN) and RHIC (Relativistic Heavy Ion Collider, Brookhaven).

In this chapter, we begin with the description of the projectile and target nuclei of the collisions defined by the UrQMD model. Then in section 2.2 we explain the potentials used in this model. Finally, at the end of this chapter we present 55 baryon species, 32 meson species and the cross section of $\bar{p}p$ collisions as the collisions term which will be used later in chapter III.

2.1 Initialization

In the UrQMD model (Bass, Belkacem, Bleicher et al., 1998; Bleicher et al., 1999), the nucleon are expressed in term of Gaussian shaped density distributions,

$$\varphi_j(\vec{x}_j, t) = \left(\frac{2\alpha}{\pi}\right)^{\frac{3}{4}} \exp\left\{-\alpha\left(\vec{x}_j - \vec{r}_j(t)\right)^2 + \frac{i}{\hbar}\vec{p}_j(t) \cdot \vec{x}_j\right\} \quad (2.1)$$

and the wave function of the nucleus are written in term of the product wave function of the single nucleon Gaussian

$$\Phi = \prod_j \varphi_j(\vec{x}_j, \vec{p}_j, t). \quad (2.2)$$

Each initialized nucleus must satisfy the following conditions:

- $\sum_i \vec{q}_i = 0$, i.e., it is concentrated in configuration space around 0
- $\sum_i \vec{v}_i = 0$, i.e., the nucleus is at rest
- its binding energy should agree with the value given by the Bethe-Weizsacker formula,
- the radius should depend on mass number

$$R(A) = r_0 \left[\frac{1}{2} \left\{ A + \left(A^{\frac{1}{3}} - 1 \right)^3 \right\} \right]^{\frac{1}{3}} \quad (2.3)$$

and have a suitable surface-thickness,

- in its center, the nucleus should have nuclear matter ground state density.

The radius r_0 is defined in term of a function of the nuclear matter ground state density (ρ_0) which is used in the UrQMD model

$$r_0 = \left(\frac{3}{4\pi\rho_0} \right)^{\frac{1}{3}}. \quad (2.4)$$

The initial momenta of the nucleons are randomly chosen from 0 to the local Thomas-Fermi-momentum

$$p_F^{\max} = \hbar c (3\pi^2 \rho)^{\frac{1}{3}} \quad (2.5)$$

where ρ is local proton density.

The interactions are included non-relativistic density-dependent Skyrme potential with additional Yukawa- and Coulomb potentials. Momentum dependent potentials are not used however Pauli-potential, may be included optionally.

2.2 Equations of motion

In this section the potentials term and kinetics term which are importance part in Hamiltonion are introduced. First, the potentials part are the Skyrme, Yukawa, Coulomb and Pauli potential. Then in the second part the complete Hamiltonion of UrQMD is given. The Eq. (2.1) gives the nucleon- or baryon-density

$$\varrho_j(\vec{x}_j, t) = \left(\frac{2\alpha}{\pi}\right)^{\frac{3}{2}} \exp\left\{-2\alpha\left(\vec{x}_j - \vec{r}_j(t)\right)^2\right\} \quad (2.6)$$

where \vec{x}_j and $\vec{r}_j(t)$ are the quantum mechanical position variable and the classical parameter of the Gaussian respectively. The Skyrme-Potential (momentum-dependence and spin-exchange has been neglected) is

$$V^{Sk} = \frac{1}{2!} t_1 \sum_{j,k} \delta(\vec{x}_i - \vec{x}_k) + \frac{1}{3!} t_2 \sum_{j,k,l} \delta(\vec{x}_j - \vec{x}_k) \delta(\vec{x}_j - \vec{x}_l) \quad (2.7)$$

where in order to exclude self-interactions, all terms where at least two indices are identical, are discarded in the primes sum. This potential composes of a sum of two- and a three-body interaction terms. The first term, which is the two-body term, is responsible for the long range attractive component of the nucleon-nucleon interaction and the second term is responsible for the short range repulsive part

of the interaction. The two-body Skyrme potential of particle j is obtained by putting Eq. (2.1) into the first term of Eq. (2.7)

$$\begin{aligned}
V_j^{Sk2} &= \sum_k^N \int d\vec{x}_j d\vec{x}_k \varphi_j^* (\vec{x}_j) \varphi_k^* (\vec{x}_k) t_1 \delta (\vec{x}_j - \vec{x}_k) \varphi_j (\vec{x}_j) \varphi_k (\vec{x}_k) \\
V_j^{Sk2} &= t_1 \sum_k^N \left(\frac{\alpha}{\pi} \right)^{\frac{3}{2}} \exp \left\{ -\alpha (\vec{r}_j - \vec{r}_k)^2 \right\} \\
V_j^{Sk2} &= t_1 \varrho_j^{\text{int}} (\vec{r}_j).
\end{aligned} \tag{2.8}$$

In the last line of Eq. (2.8), the interaction density was introduced. It has the same form as nucleon density (2.6) which is obtained from the Wigner-transform of the Gaussian (2.1), but omits the nucleon at the location j and its Gaussian has twice the width of that used in equation (2.6). The three-body potential for particle j can be obtained in the same way as Eq. (2.8)

$$\begin{aligned}
V_j^{Sk3} &= \frac{1}{2!} \sum_{kl}^N \int d\vec{x}_j d\vec{x}_k d\vec{x}_l \varphi_j^* (\vec{x}_j) \varphi_k^* (\vec{x}_k) \varphi_l^* (\vec{x}_l) \\
&\quad \times t_2 \delta (\vec{x}_j - \vec{x}_k) \delta (\vec{x}_j - \vec{x}_l) \varphi_j (\vec{x}_j) \varphi_k (\vec{x}_k) \varphi_l (\vec{x}_l) \\
V_j^{Sk3} &= t_2 \frac{1}{2!} \sum_{kl}^N \left(\frac{4\alpha^2}{3\pi^2} \right)^{\frac{3}{2}} \\
&\quad \times \exp \left\{ -\frac{2}{3} \alpha \left((\vec{r}_j - \vec{r}_k)^2 + (\vec{r}_k - \vec{r}_l)^2 + (\vec{r}_l - \vec{r}_j)^2 \right) \right\}.
\end{aligned} \tag{2.9}$$

From the Eq. (2.9), if we considered the infinite nuclear matter case, the individual relative distances should approximately equal to their average value. Therefore, the relative distance of particle k and l may be replaced by the average of the other two relative distances

$$V_j^{Sk3} \approx t_2 \frac{1}{2!} \sum_{kl}^N \left(\frac{4\alpha^2}{3\pi^2} \right)^{\frac{3}{2}} \exp \left\{ -\alpha \left((\vec{r}_j - \vec{r}_k)^2 + (\vec{r}_l - \vec{r}_j)^2 \right) \right\}. \tag{2.10}$$

Eq. (2.10) can be rewritten as Eq. (2.11) using the definition of interaction density from Eq. (2.8).

$$V_j^{Sk3} \approx t_2 3^{-\frac{3}{2}} (\varrho_j^{\text{int}})^2. \tag{2.11}$$

The differences between Eq. (2.8) and (2.11) are the coefficient and the power of the interaction density term.

$$V_j^{Sk3} \approx t_\gamma (\gamma + 1)^{-\frac{3}{2}} (\rho_j^{\text{int}})^\gamma. \quad (2.12)$$

Expression (2.12) is a generalized form of the three body interaction. It is always used in the UrQMD model. When $\gamma=2$, the equation above turns to the interaction of three body term.

The Yukawa-, Coulomb-, and (optional) Pauli potential can be written in term of two-body interactions which are shown in Eq. (2.13), (2.14) and (2.15), respectively.

$$V_{Yuk}^{ij} = V_0^{Yuk} \frac{\exp \left\{ - \left| \vec{r}_i - \vec{r}_j \right| / \gamma_Y \right\}}{\left| \vec{r}_i - \vec{r}_j \right|} \quad (2.13)$$

$$V_{Coul}^{ij} = \frac{Z_i Z_j e^2}{\left| \vec{r}_i - \vec{r}_j \right|} \quad (2.14)$$

$$V_{Pau}^{ij} = V_{Pau}^0 \left(\frac{\hbar}{q_0 p_0} \right)^3 \exp \left\{ - \frac{\left| \vec{r}_i - \vec{r}_j \right|^2}{2q_0^2} - \frac{\left| \vec{p}_i - \vec{p}_j \right|^2}{2p_0^2} \right\} \delta_{\tau_i \tau_j} \delta_{\sigma_i \sigma_j} \quad (2.15)$$

where γ_Y is a parameter given in Table (2.1), Z_j represents its charge, τ_j is isospin and σ_j is the spin of particle j .

For the infinite nuclear matter, the contribution of the Yukawa-potential for the total energy has a linear density-dependence same as the two-body Skyrme-contribution. As a result all parameter sets which satisfy the following relation for the parameter t_1 yield the same equation of state in infinite nuclear matter

$$\frac{1}{2} t_1 + 2\pi V_0^{Yuk} \gamma_Y^2 = \text{const.} \quad (2.16)$$

For finite nuclei, the parameter of Yukawa potential are the same without changing the equation of state.

Finally, we get the classical UrQMD Hamiltonian which covers the motion of the parameters, \vec{r}_j and \vec{p}_j , of the wave-functions as

$$H_{UrQMD} = \sum_{j=1}^N E_j^{kin} + \frac{1}{2} \sum_{j=1}^N \sum_{k=1}^N (E_{jk}^{Sk2} + E_{jk}^{Yukawa} + E_{jk}^{Coulomb} + E_{jk}^{Pauli}) + \frac{1}{6} \sum_{j=1}^N \sum_{k=1}^N \sum_{l=1}^N E_{jkl}^{Sk3} \quad (2.17)$$

where the kinetics term is

$$E_j^{kin} = \sqrt{p_j^2 + m_j^2} \quad (2.18)$$

and the two body Skyrme is

$$E_{jk}^{Sk2} = t_1 \left(\frac{\alpha}{\pi} \right)^{\frac{3}{2}} \exp \{ -\alpha r_{jk}^2 \} \quad (2.19)$$

and the three body Skyrme is

$$E_{jkl}^{Sk3} = t_\gamma \left(\frac{4\alpha^2}{3\pi^2} \right)^{\frac{3}{2}} \exp \{ -\alpha (r_{jk}^2 + r_{jl}^2) \}. \quad (2.20)$$

The Yukawa potential is

$$E_{jk}^{Yukawa} = V_0^{Yuk} \frac{1}{2r_{jk}} \exp \left\{ \frac{1}{4\alpha\gamma_Y^2} \right\} \times \left[\exp \left\{ -\frac{r_{jk}}{\gamma_Y} \right\} \left(1 - \text{erf} \left(\frac{1}{2\gamma_Y\sqrt{\alpha}} - \sqrt{\alpha}r_{jk} \right) \right) - \exp \left\{ \frac{r_{jk}}{\gamma_Y} \right\} \left(1 - \text{erf} \left(\frac{1}{2\gamma_Y\sqrt{\alpha}} + \sqrt{\alpha}r_{jk} \right) \right) \right] \quad (2.21)$$

and the Coulomb potential is

$$E_{jk}^{Coulomb} = \frac{Z_i Z_j e^2}{r_{jk}} \text{erf}(\sqrt{\alpha}r_{jk}) \quad (2.22)$$

and the Pauli potential is

$$E_{jk}^{Pauli} = V_{Pau}^0 \left(\frac{\hbar}{p_0 q_0} \right)^3 \left(1 + \frac{1}{2\alpha q_0^2} \right)^{-\frac{3}{2}} \times \exp \left\{ -\frac{\alpha r_{jk}^2}{2\alpha q_0^2 + 1} - \frac{p_{jk}^2}{2p_0^2} \right\} \delta_{\tau_j \tau_k} \delta_{\sigma_j \sigma_k} \quad (2.23)$$

Table 2.1: Parameters of the hard equation of state implemented in the UrQMD model, with and without Pauli-potential.

parameter	without Pauli-potential	with Pauli-potential
$\alpha(fm^{-2})$	0.25	0.1152
$t_1(MeVfm^3)$	-7264.04	-84.5
$t_\gamma(MeVfm^6)$	87.65	188.2
γ	1.675	1.46
$V_0^{Yukawa}(MeVfm)$	-0.498	-85.1
γ_Y	1.4	1.0
$V_0^{Pauli}(MeV)$	-	98.95
$q_0(fm)$	-	2.16
$p_0(MeV/c)$	-	120

with

$$r_{jk} = \left| \vec{r}_j - \vec{r}_k \right| \quad (2.24)$$

and

$$p_{jk} = \left| \vec{p}_j - \vec{p}_k \right|. \quad (2.25)$$

In the UrQMD model only hard equation of state has been implemented and all parameters used are listed in Table (2.1). At present the generalization of two body forces to the relativistic region is not fully incorporated.

2.3 The collision term

In each collisions, there are many kinds of particle being produced. The UrQMD model has capability to identify 55 different of baryon species (including

nucleon, delta, hyperon and their resonances) which masses up to $2.25 \text{ GeV}/c^2$ and 32 different of meson species (including strange meson and its resonances). But their anti-particle and isospin-projected states can also be determined. Table (2.2) shows 6 type of baryon and their corresponding masses which can be found in the UrQMD. In Table (2.3), meson and meson resonance, arranged by their spin and parity are given.

One of the most importance of baryon-antibaryon interactions is the total cross-section which comes from the process of annihilation when energies $p_{lab} = 100 \text{ GeV}/c$. The earlier experiments on $\bar{p}p$ -annihilation revealed a number of differences from the non-annihilation channels. It is not fully understood whether they come from the kinematic restrictions on the available phase space, or related to dynamical differences between the non-annihilation and annihilation mechanisms. In the experimental results (Zabrodin et al., 1995) the comparison between pp interactions and non-annihilation $\bar{p}p$ interactions at $32 \text{ GeV}/c$ supported the conclusion of equivalence of pp interaction and non-annihilation $\bar{p}p$ interaction processes.

The UrQMD parameters are obtained from fitting the experimental data. For $\bar{p}p$ cross section, the data from Barnett's experiment (Barnett et al., 1996) are used. Fig. (2.1) shows the UrQMD parameterizations comparing to the experiment (Barnett et al., 1996). The total $\bar{p}p$ cross-sections correspond to a solid line. The annihilation cross-sections are exhibited by a dash line and elastic cross-sections are represented by a dot line.

In UrQMD model the $\bar{p}p$ total and elastic cross section derive from the CERN/HERA parameterizations and the annihilation cross section come from the Koch and Dover parameterizations.

Table 2.2: Baryons and baryon-resonances included into the UrQMD model. Through baryon-antibaryon symmetry the respective antibaryon states are included as well.

Nucleon	Delta	Lambda	Sigma	Xi	Omega
N_{938}	Δ_{1232}	Λ_{1116}	Σ_{1192}	Ξ_{1315}	Ω_{1672}
N_{1440}	Δ_{1600}	Λ_{1405}	Σ_{1385}	Ξ_{1530}	
N_{1520}	Δ_{1620}	Λ_{1520}	Σ_{1660}	Ξ_{1690}	
N_{1535}	Δ_{1700}	Λ_{1600}	Σ_{1670}	Ξ_{1820}	
N_{1650}	Δ_{1900}	Λ_{1670}	Σ_{1750}	Ξ_{1950}	
N_{1675}	Δ_{1905}	Λ_{1690}	Σ_{1775}	Ξ_{2030}	
N_{1680}	Δ_{1910}	Λ_{1800}	Σ_{1915}		
N_{1700}	Δ_{1920}	Λ_{1810}	Σ_{1940}		
N_{1710}	Δ_{1930}	Λ_{1820}	Σ_{2030}		
N_{1720}	Δ_{1950}	Λ_{1830}			
N_{1900}		Λ_{1890}			
N_{1990}		Λ_{2100}			
N_{2080}		Λ_{2110}			
N_{2190}					
N_{2200}					
N_{2250}					

Table 2.3: Mesons and meson-resonances, sorted with respect to spin and parity, included into the UrQMD model.

0^{-+}	1^{--}	0^{++}	1^{++}	1^{+-}	2^{++}	$(1^{--})^*$	$(1^{--})^{**}$
π	ρ	a_0	a_1	b_1	a_2	ρ_{1450}	ρ_{1700}
K	K^*	K_0^*	K_1^*	K_1	K_2^*	K_{1410}^*	K_{1680}^*
η	ω	f_0	f_1	h_1	f_2	ω_{1420}	ω_{1662}
η'	ϕ	f_0^*	f_1'	h_1'	f_2'	ϕ_{1680}	ϕ_{1900}

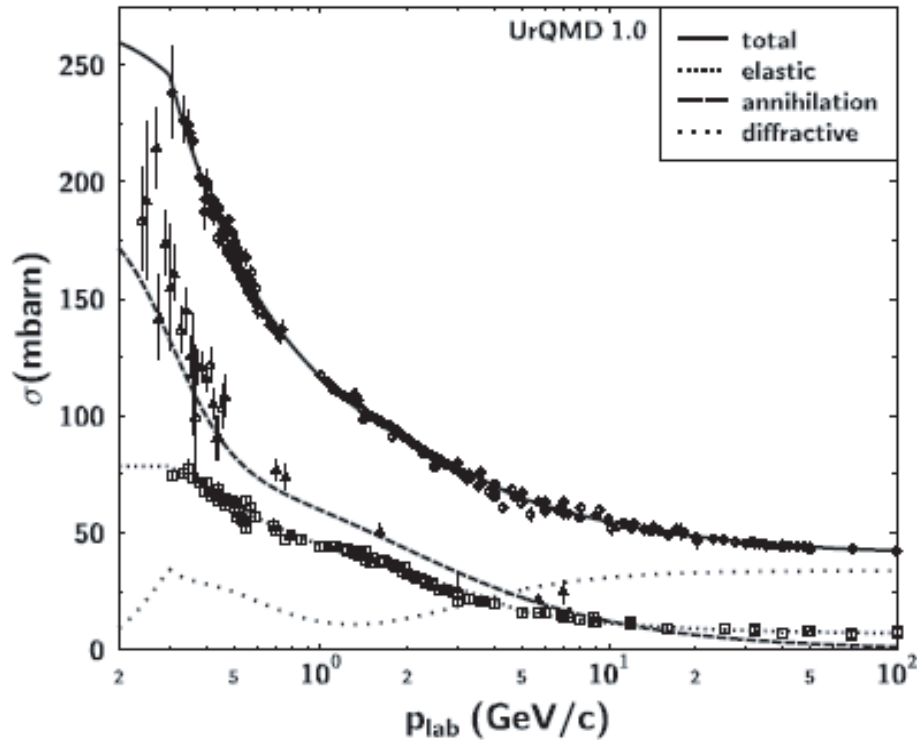


Figure 2.1: The $\bar{p}p$ cross-section as compared to the experimental data (Barnett et al., 1996) on total (open circles), elastic (open squares), and annihilation (open triangles) cross-sections. The diffractive cross-section is assumed to be a difference between the total cross-section and the sum of the elastic and annihilation cross-section.

Table 2.4: Parameters for the CERN/HERA parameterization for the total and elastic antiproton -proton cross-sections. This parameterization is used in UrQMD for momenta $p_{lab} > 5\text{GeV}/c$.

σ	A	B	C	D	n
total	38.4	77.6	0.26	-1.2	-0.64
elastic	10.2	52.7	0.125	-1.28	-1.16

The total and elastic $\bar{p}p$ cross-sections is given by

$$\sigma(p) = A + Bp^n + C \ln^2(p) + D \ln(p) \quad (2.26)$$

where p represents the laboratory-momentum in unit of GeV/c , σ represents the cross-section in unit of millibarn (mb). A, B, C and D are parameters which are some number show in Table (2.4).

For $p_{lab} < 5\text{GeV}/c$, UrQMD uses another parameterization to obtain the total and elastic cross section which are shown in Eq. (2.27) and (2.28), respectively.

$$\sigma_{tot}(p) = \begin{cases} 75.0 + 43.1p^{-1} + 2.6p^{-2} - 3.9p & : 0.3 < p < 5 \\ 271.6 \exp(-1.1p^2) & : p < 0.3 \end{cases} \quad (2.27)$$

$$\sigma_{el}(p) = \begin{cases} 31.6 + 18.3p^{-1} - 1.1p^{-2} - 3.8p & : 0.3 < p < 5 \\ 78.6 & : p < 0.3 \end{cases} \quad (2.28)$$

The $\bar{p}p$ annihilation cross-section is given by Koch and Dover (Koch and Dover, 1989)

$$\sigma_{ann}^{\bar{p}p} = \sigma_0^N \frac{s_0}{s} \left[\frac{A^2 s_0}{(s - s_0)^2 + A^2 s_0} + B \right] \quad (2.29)$$

where $\sigma_0^N = 120 \text{ mb}$, $s_0 = 4m_N^2$, $A=50 \text{ MeV}$ and $B=0.6$.

In theory, the sum of annihilation and elastic cross-sections should be equal to the total cross-section. However, from experiment, the sum of annihilation and elastic cross-sections is smaller than the total cross section

$$\Delta\sigma = \sigma_{tot} - \sigma_{el} - \sigma_{ann} \quad (2.30)$$

The value of $\Delta\sigma$ is interpreted as the diffractive cross-section which describes the excitation at least one of the collision particles to a resonance or to a string via Pomeron exchange.

In this chapter, some details of UrQMD model are described only the wave function of nucleon, the Hamiltonion term and the collisions term of antibaryon-baryon system. To confirm that we are able to use the model effectively, the calculations between UrQMD and experimental data are compared in chapter III.

CHAPTER III

NUMERICAL CALCULATIONS

To check that our Nucleus-Nucleus calculations are correct, we compare the results with the Nucleus-Nucleus Collisions at High Baryon Densities (Weber, Bratkovskaya and Stoecker, 2002) and the Energy dependence of pion and kaon production in central Pb+Pb collisions (Afanasiev, Anticic et al., 2002). The detail comparisons are shown in section 3.1. For Baryon-Baryon interactions, we verify our calculations with the Strangeness dynamics and transverse pressure in relativistic nucleus-nucleus collisions (Bratkovskaya, Bleicher, Reiter, Soff, Stoecker, Leeuwen, Bass and Cassing, 2004) and give the details in section 3.2.

Before starting the section 3.1, we shall introduce a brief definition of some quantities which will be used later in section 3.1 and 3.2. The first quantity is rapidity (y). We define the rapidity as

$$y = \frac{1}{2} \ln \left(\frac{E + p_z}{E - p_z} \right) \quad (3.1)$$

where E is the relativistic energy $E = \sqrt{p^2 + m^2}$, and p_z is the momentum in \hat{z} direction.

Secondly, we define the rapidity distribution (dN/dy) as a number of particles per unit rapidity with respect to rapidity.

Next, we use $m_t = \sqrt{p_t^2 + m^2}$ as the transverse mass where p_t is the transverse momentum $p_t = \sqrt{p_x^2 + p_y^2}$, and m is the mass of considered particles.

The last quantity which we will define here is the percent of particle yields. It is a number of considered particles multiply by 100 and divide by the number

of total particles.

3.1 $Pb + Pb$ Interactions

NA49 is a large acceptance tracking spectrometer at the European Organization for Nuclear Research (CERN) Super Proton Synchrotron accelerator (SPS) Lead beam facility. By identifying charged hadrons and neutral strange particles it investigates hadronic signals of plasma formation and does hadron "thermometry". The NA49 experimental setup (Afanasiev et al., 1999) is shown in Fig. (3.1). It has been used in studying the production of charged hadrons ($\pi^\pm, K^\pm, p, \bar{p}$), and neutral strange particles ($K^0, \Lambda, \bar{\Lambda}$), in a search for the deconfinement transition predicted by lattice QCD. The experiment is designed to use two large volume, fine granularity Time Projection Chambers (TPC's), and two intermediate size TPC's for vertex tracking of neutral strange particle decays.

The measurements of NA49 Collaboration give the results of $Pb + Pb$ collisions at 40, 80 and 160 AGeV (Afanasiev, Anticic et al., 2002). The data are shown in the Fig. (3.2) and the parameters are given in Table (3.1).

In Fig. (3.2), the solid lines come from rapidity spectra

$$\frac{dN}{dy} = N \left[\exp \left(-\frac{(y - y_0)^2}{2\sigma^2} \right) + \exp \left(-\frac{(y + y_0)^2}{2\sigma^2} \right) \right]. \quad (3.2)$$

which are parametrized by the sum of two Gauss (2-G) distributions placed symmetrically with respect to midrapidity.

We obtain the values of parameters N, y_0 and σ from Table (3.1). When the incoming energies increase, both y_0 and σ increase and the width of the observed rapidity distributions is also increase.

In 2002, Weber, Bratkovskaya and Stoecker (Weber, Bratkovskaya and Stoecker, 2002) have studied most central collision of $Pb+Pb$ at 20, 40, 80 and 160

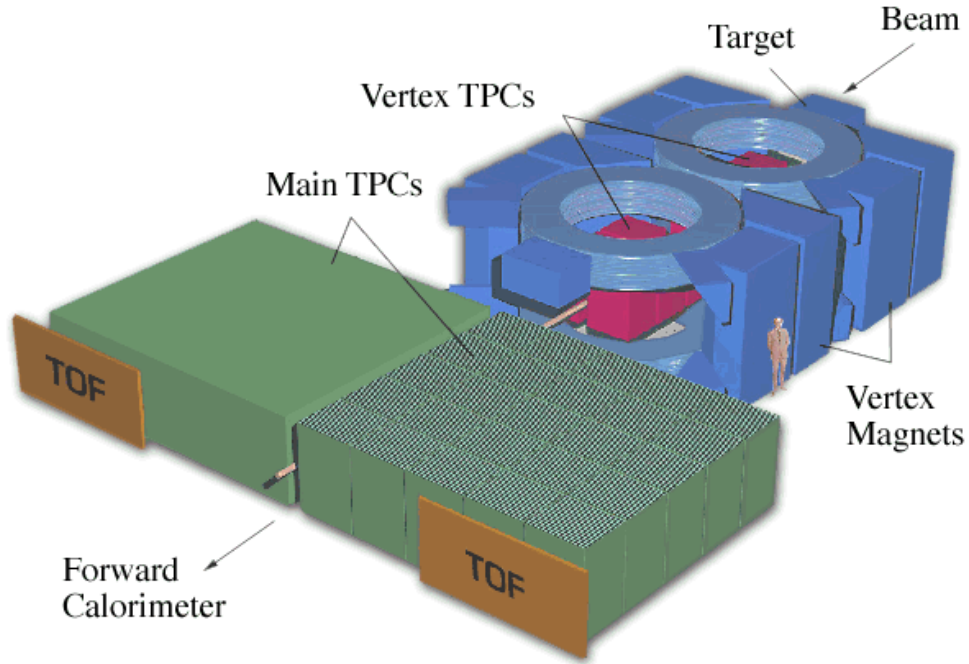


Figure 3.1: The NA49 experimental setup. (Available: <http://na49info.cern.ch/>)

AGeV using the UrQMD model and compare rapidity distributions of π^- , K^+ , K^- and Λ with the measurements from the NA49 Collaboration. They have found that the UrQMD model describes the data reasonably, but overpredicts the π^- yield by $\sim 20\%$, whereas the K^+ yield is underestimated by $\sim 15\%$. The K^- yields are in a good agreement with the experimental data, and the Λ yields are also in a reasonable correspondence with the data for all energies.

Before showing our results, it is instructive to look at the word *most central*. The most central is the quantity that tell us how big impact parameter (b) used in the collisions, it also known as centrality (c) (Broniowski and Florkowski, 2002). The centrality is defined as the percentile of events with the largest number of produced particles (as registered in detectors), or the largest number of participants. The impact parameter is in a sense more basic, since it determines the

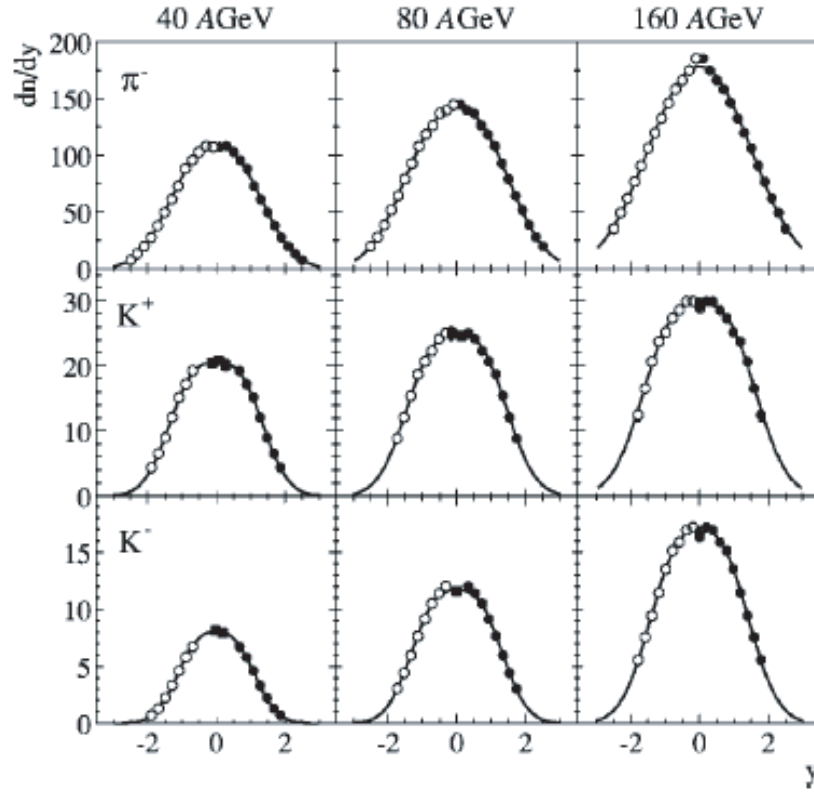


Figure 3.2: Rapidity distributions of π^- , K^+ and K^- mesons produced in central $Pb + Pb$ collisions at 40, 80 and 160 AGeV. The closed symbols indicate measured points, open points are reflected with respect to midrapidity. The lines indicate 2-G fits to spectra [see Eq.(3.2)].

Table 3.1: Fitted parameters of the 2-G parametrization of rapidity distributions measured for π^- , K^+ , K^- mesons produced in central $Pb + Pb$ collisions at 40, 80 and 160 AGeV.

	40 AGeV	80 AGeV	160 AGeV
$N(\pi^-)$	74.0 ± 0.5	97.0 ± 0.7	107.6 ± 1.8
$N(K^+)$	16.2 ± 0.4	19.3 ± 0.3	23.4 ± 0.6
$N(K^-)$	6.03 ± 0.13	9.16 ± 0.12	12.8 ± 0.3
$\sigma(\pi^-)$	0.872 ± 0.005	0.974 ± 0.007	1.18 ± 0.02
$\sigma(K^+)$	0.725 ± 0.016	0.792 ± 0.018	0.88 ± 0.04
$\sigma(K^-)$	0.635 ± 0.011	0.705 ± 0.010	0.81 ± 0.02
$y_0(\pi^-)$	0.666 ± 0.006	0.756 ± 0.006	0.72 ± 0.02
$y_0(K^+)$	0.694 ± 0.008	0.742 ± 0.008	0.839 ± 0.012
$y_0(K^-)$	0.569 ± 0.010	0.668 ± 0.005	0.727 ± 0.010

initial geometry of the collision and appears across the formalism. Theoreticians need to assign an impact parameter to a given centrality. In relativistic heavy-ion collisions, the geometric relation of centrality to the impact parameter is defined by

$$c \simeq \frac{\pi b^2}{\sigma_{inel}} \quad for \quad b < \bar{R}, \quad (3.3)$$

where σ_{inel} is the total inelastic nucleus-nucleus cross section and \bar{R} is the order of the sum of the radii of the colliding nuclei.

For example, to understand how big impact parameter of 7% central $Pb + Pb$ collisions. We would like to explain how to get impact parameter so we put $c = 0.07$ (7%) and $\sigma_{inel} = 7.15$ barn (Afanasiev, Anticic et al., 2002) into Eq.

(3.3) where 1 barn= 100 fm^2 ,

$$\begin{aligned}
 c &= \frac{\pi b^2}{\sigma_{inel}} \\
 b &= \sqrt{\frac{c\sigma_{inel}}{\pi}} \\
 b &= \sqrt{\frac{0.07 \times 7.15 \times 100 fm^2}{3.14}} \\
 b &= 3.99 fm
 \end{aligned}$$

We get, 7% and 5% central $Pb+Pb$ collisions which are corresponding to $b < 3.99$ fm and $b < 3.37$ fm respectively.

In this thesis, we study most central collision of $Pb+Pb$ at 40, 80 and 160 AGeV using the UrQMD model version 1.3 and compare the rapidity distributions of π^- , K^+ and K^- with the results from the NA49 Collaboration.

The comparisons of UrQMD version 1.3 calculations for the most central (7% and 5%) $Pb+Pb$ collisions at 40, 80 and 160 AGeV with the data from NA49 Collaboration are shown in the Fig. (3.3) for π^- , K^+ and K^- . We have found that the UrQMD version 1.3 calculations are in a good agreement with the experimental data.

3.2 $p+p$ Interactions

To confirm that our baryon-baryon calculations are corrected, we calculate $p+p$ collisions within UrQMD model version 1.3 and compare our results with the experimental data from NA49 (Kraus, 2004) and STAR Collaborations (Ackermann et al., 1999).

From NA49 (Kraus, 2004) we obtain the inverse slope parameter (T) . The relation between inverse slope and transverse mass spectra at midrapidity is

$$\frac{d^2 N}{m_t \cdot dy \cdot dm_t} \sim e^{-m_t/T} \quad (3.4)$$

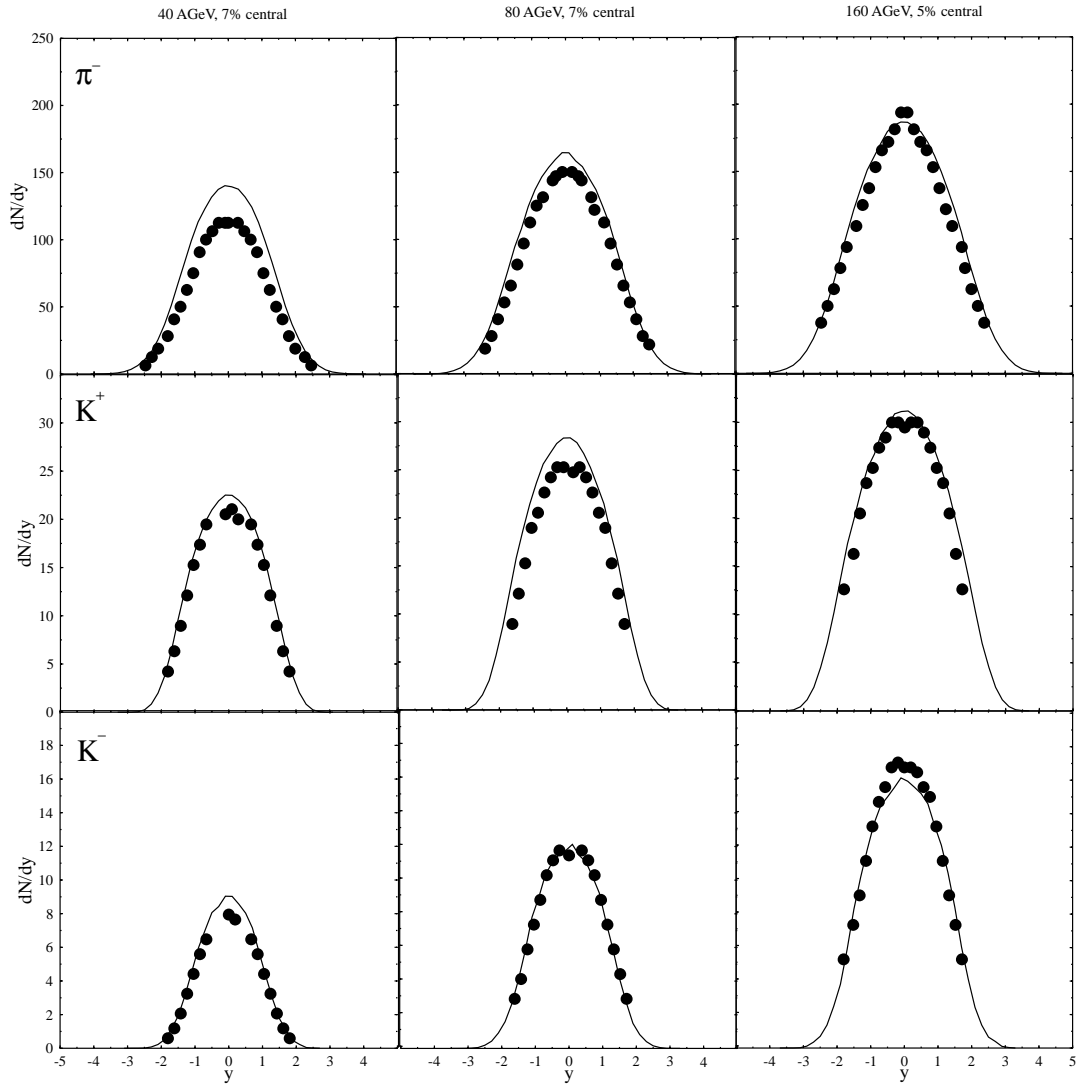


Figure 3.3: The rapidity distribution of π^- , K^+ and K^- in 7% or 5% central $Pb + Pb$ collisions at 40, 80 and 160 AGeV calculated within the UrQMD model (solid lines) version 1.3 in comparison with the experimental data from the NA49 Collaboration at 40, 80 and 160 AGeV (the symbol represent π^- , K^+ and K^- experimental data).

where m_t is transverse mass, y is rapidity and N is a number of considered particles.

In our calculations, we get the transverse mass for pions and kaons. Then we compare our results with the results from NA49. The logarithmic plot between transverse mass distribution and transverse mass of considered particles is displayed in Fig. (3.4).

The thin lines correspond to fits with the experimental slope parameters 163 ± 10 MeV for π^- , 172 ± 17 MeV for K^+ and 164 ± 16 MeV for K^- from Ref. (Kraus, 2004). The long dashed line, dot line and dashed line represent the transverse mass spectra at midrapidity for π^- , K^+ and $K^-(\times 0.1)$ respectively. We have found that our calculations are in good agreement with the experimental data from NA49.

Next, we compare the experimental data of $p + p$ collisions at $\sqrt{s}=200$ GeV from STAR collaboration (Ackermann et al., 1999). In this case, the STAR collaboration give us the data of transverse mass distribution for π^- and K^- which can be compare directly to our calculations.

The comparison of STAR results with the UrQMD results are shown in Fig. (3.5). The full symbols indicate the data from the STAR Collaboration (Barannikova and Wang, 2003). The dot and dashed line represent the transverse mass spectra at midrapidity for π^- and K^- respectively. It can be seen clearly that the transverse mass spectra for both π^- and K^- are almost the same.

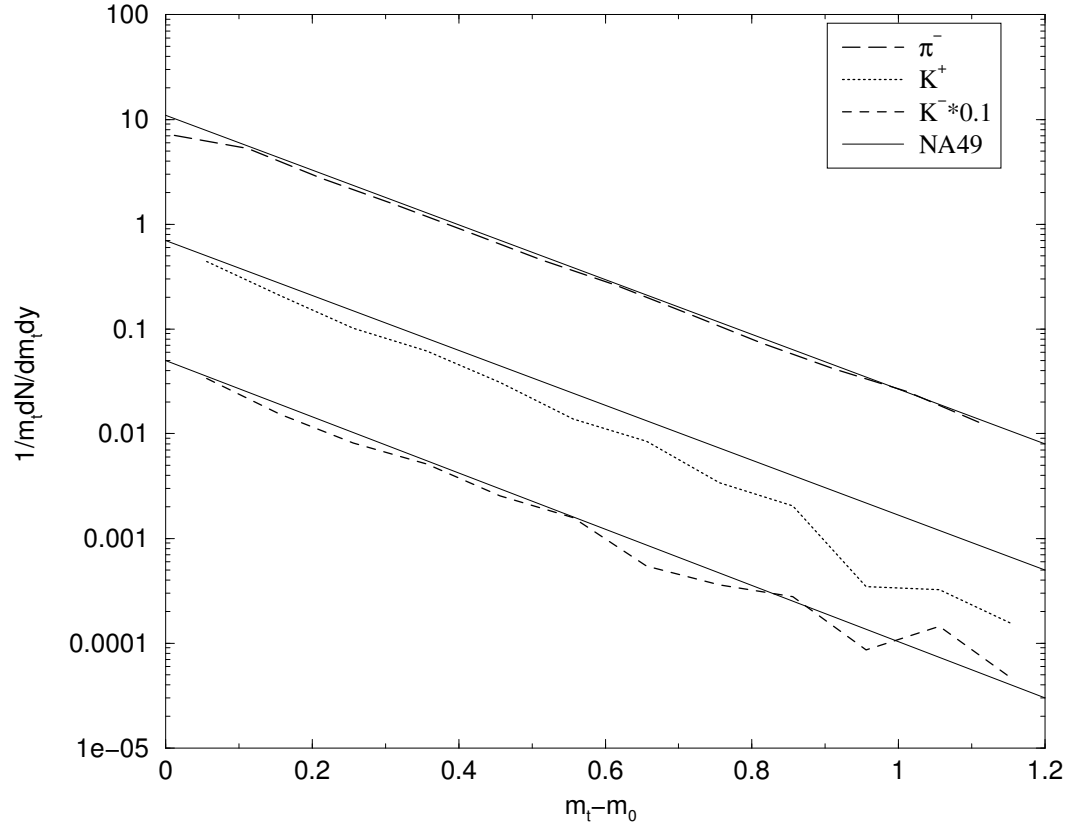


Figure 3.4: The transverse mass spectra at midrapidity for π^- , K^+ and $K^-(\times 0.1)$ (long dashed line, dot line and dashed line respectively) from $p + p$ reactions at 160 GeV from UrQMD version 1.3. The thin lines correspond to fits of experimental slope parameters from NA49 (Kraus, 2004).

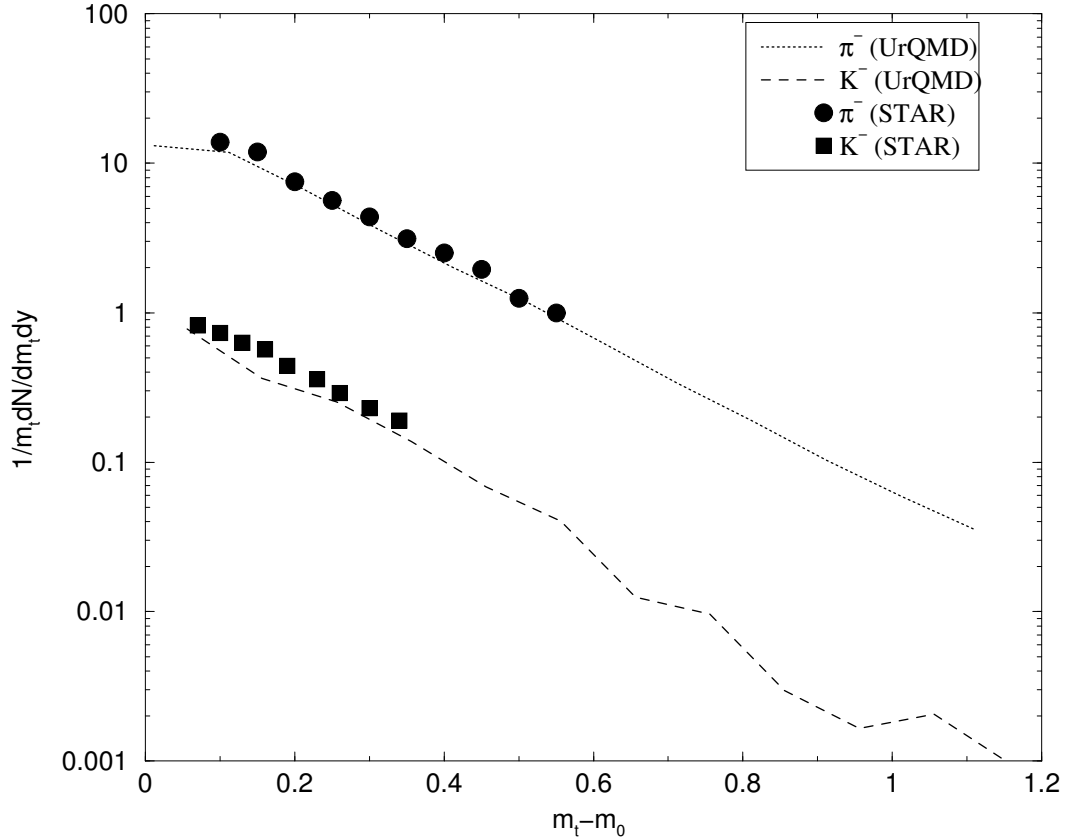


Figure 3.5: The transverse mass spectra at midrapidity for π^- and K^- from $p + p$ reactions at $\sqrt{s} = 200$ GeV from UrQMD version 1.3 (dot and dashed lines, multiplied by a factor of 2). The square and dot symbols indicate the data from the STAR Collaboration (Barannikova and Wang, 2003).

From section 3.1 and 3.2, we have successfully shown that our calculations using UrQMD model version 1.3 in the collisions of nucleus-nucleus and baryon-baryon, are in good agreement with the experimental data from NA49 and STAR collaboration. This evidence confirm that we can use the UrQMD model to calculate the interaction between nucleus-nucleus and baryon-baryon correctly.

In next chapter, we will apply this method to calculate $\bar{p} + p$ interactions in order to study the particles yield and rapidity distribution of $p, \bar{p}, n, \bar{n}, \pi^0, \pi^+, \pi^-, K^+, K^-, K^0$ and \bar{K}^0 at energy range from 20 up to 160 GeV.

CHAPTER IV

RESULTS AND DISCUSSIONS

In this chapter we investigate the $\bar{p} + p$ collisions in the UrQMD model with 2,000,000 events simulated. Predictions are given for the particle yields, the rapidity distribution and transverse mass distribution of particles at center-of-mass energies $\sqrt{s} = 20, 40, 80$ and 160 GeV. The impact parameter employed in our study is smaller than 0.87 fm, which is the charge radius of proton.

4.1 Particle Yields

It is found that the total particle yields increase slightly when the center-of-mass energy is raised from 20 GeV to 160 GeV. The total particle yields per event are 5.55, 5.61, 5.75 and 5.87 for the energies $\sqrt{s} = 20, 40, 80$ and 160 GeV, respectively. Shown in Table (4.1) and Table (4.2) are respectively the yields per event for various individual particles and the corresponding ratios with respect to the total yields. The yield ratios averaged over all the energies considered are listed in the last column of Table (4.2).

Table (4.1) and Table (4.2) show that the pion mesons have the highest yields while the kaons are produced with very lower productions. Averaged over all the energies, we have 61.61% for pion yield and 1.99% for kaon yield. The production of other particles except for the ones listed in Table (4.1) and Table (4.2) has a ratio of about 1.5%. Among those particles are K_L^0 , K_s^0 , K^* , Λ and Σ . The protons and antiprotons in the final states are mainly from the elastic

Table 4.1: Particle yields per event.

\sqrt{s} (GeV)	20	40	80	160
p	0.623	0.629	0.632	0.636
\bar{p}	0.555	0.571	0.582	0.591
n	0.345	0.361	0.368	0.369
\bar{n}	0.419	0.426	0.425	0.422
π^+	1.094	1.107	1.146	1.176
π^-	1.168	1.172	1.203	1.229
π^0	1.160	1.161	1.194	1.224
K^+	0.030	0.029	0.033	0.038
K^-	0.024	0.023	0.027	0.031
K^0	0.025	0.025	0.028	0.036
\bar{K}^0	0.024	0.023	0.027	0.031

Table 4.2: Ratios of yields for individual particles.

\sqrt{s} (GeV)	20	40	80	160	Average
p	11.22	11.21	10.98	10.83	11.06
\bar{p}	10.01	10.19	10.12	10.06	10.09
n	6.22	6.44	6.40	6.29	6.33
\bar{n}	7.56	7.59	7.39	7.18	7.44
π^+	19.71	19.75	19.92	20.03	19.85
π^-	21.05	20.90	20.92	20.93	20.95
π^0	20.91	20.71	20.77	20.84	20.81
K^+	0.54	0.53	0.58	0.65	0.57
K^-	0.44	0.42	0.47	0.53	0.46
K^0	0.45	0.44	0.49	0.56	0.49
\bar{K}^0	0.43	0.41	0.47	0.53	0.46
Total	98.53	98.59	98.52	98.42	98.52

collision, which can be seen clearly from the rapidity distributions (see the next section). The neutrons and antineutrons are mainly produced by the processes $\bar{p}p \rightarrow \bar{n}n$ (charge-exchange reaction) and $\bar{p}p \rightarrow \bar{n}n\pi^0$.

In this study it is difficult to tell whether the low yield of the mesons K^+, K^-, K^0 and \bar{K}^0 is due to the low production of the strange quark in the $\bar{p}p$ collision or just obeys the statistical rule which link the production rate to the mass of a particle, that is $N \sim e^{-M/kT}$, where M is the mass of a meson, T the temperature and k the Boltzmann constant. The two different courses stem from totally different physics. It should be a very interesting topic to investigate the physics which leads to the low production of K mesons.

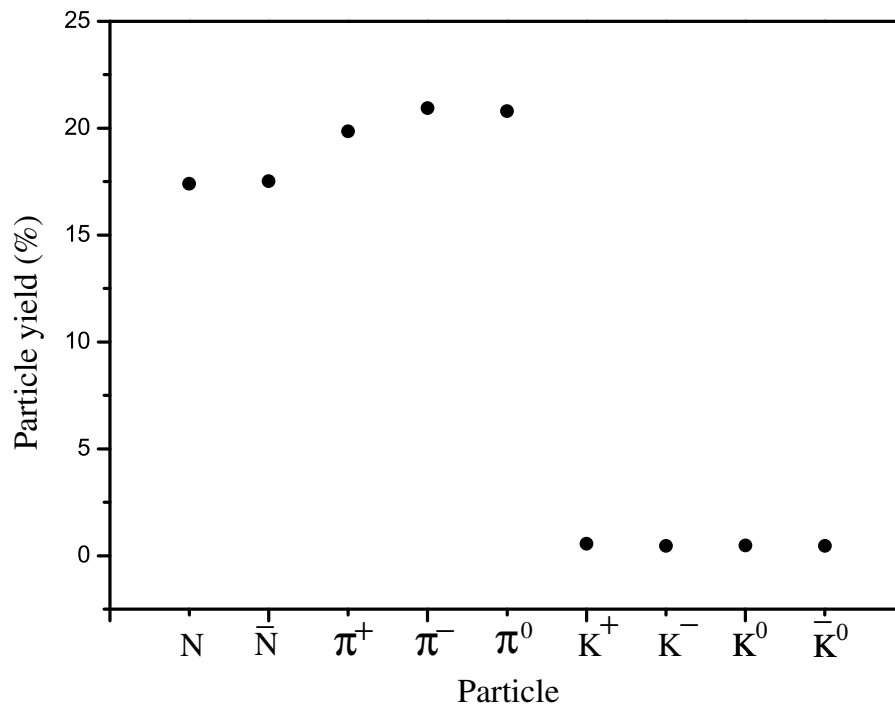


Figure 4.1: Particle yields ratios for nucleon, antinucleon, pions and kaons.

Shown in Fig. (4.1) is the yield ratios of nucleon (N), antinucleon (\bar{N}), pions and kaons. It is found that N ($p + n$) yields ratios are close to \bar{N} ($\bar{p} + \bar{n}$)

yields ratios, which is consistent with the baryon conservation law.

4.2 Rapidity distribution

In this section we study the rapidity distribution of final particles in the $\bar{p}p$ collision. Shown in Fig. (4.2) to Fig. (4.12) are the rapidity distributions for $p, \bar{p}, \pi^0, \pi^+, \pi^-, n, \bar{n}, K^+, K^-, K^0$ and \bar{K}^0 , respectively.

The peaks of the rapidity distributions of p and \bar{p} shown respectively in Fig.(4.2) and Fig.(4.3) correspond to p and \bar{p} resulting from the $p\bar{p}$ elastic collision. The p and \bar{p} which are created in the $p\bar{p}$ collision distribute mainly in the low rapidity region with $|y| < 2$. Note that the negative rapidity (y) indicates the the direction of the incoming p while the positive rapidity indicates the direction of the incoming \bar{p} .

Shown in Fig. (4.4) are the rapidity distributions of the π^0 meson. It is found that the distributions are symmetric and a large number of the π^0 meson is created around $y = 0$. A small y means that the particles are created either with a small momentum or they squeeze out in the plain of p_x and p_y . With increasing the center of mass energy, more and more π^0 are created with higher energies.

The π^+ and π^- rapidity distributions are shown in Fig. (4.5) and Fig. (4.6), respectively. The distributions are not symmetric, but more π^+ and π^- are created in the p and \bar{p} directions, respectively. The higher the center-of-mass energies, the less symmetric the distributions.

Presented in Fig. (4.7) and Fig. (4.8) are the rapidity distributions of n and \bar{n} , respectively. One may conclude that the n and \bar{n} are mainly created in the charge-exchange process $p\bar{p} \rightarrow n\bar{n}$ and the reaction $p\bar{p} \rightarrow n\bar{n}\pi^0$ for the n and \bar{n} distribute only in the p and \bar{p} directions, respectively.

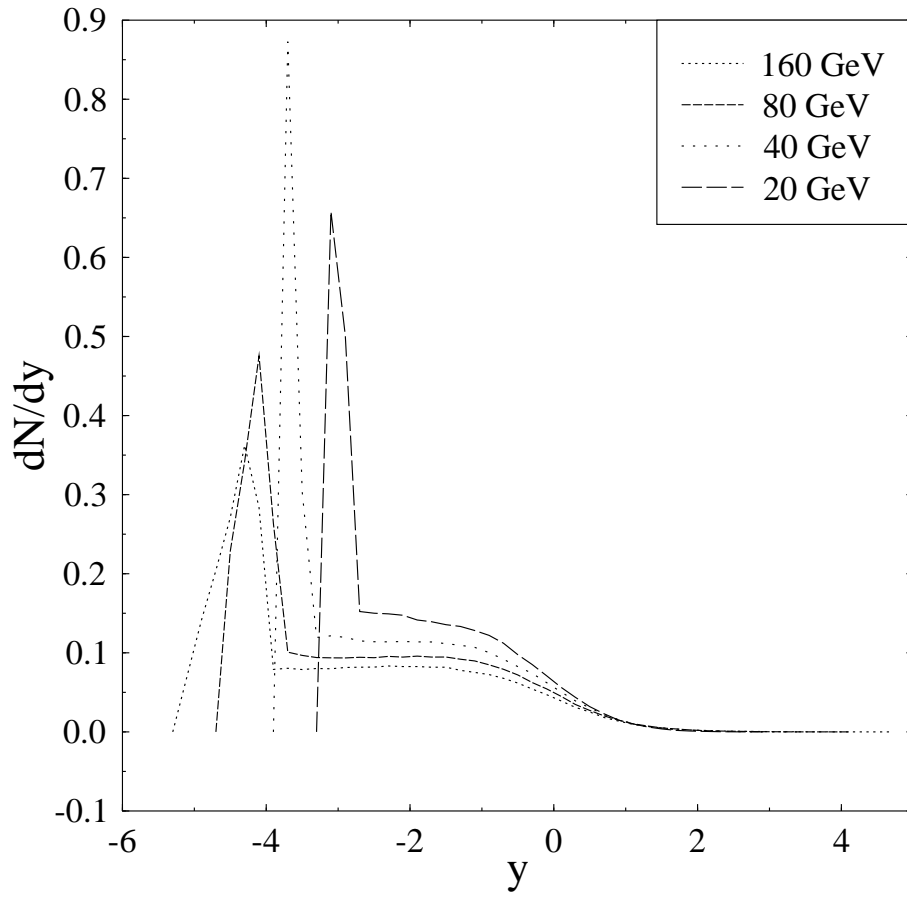


Figure 4.2: The rapidity distribution of p in $\bar{p}+p$ collisions at $\sqrt{s} = 20, 40, 80$ and 160 GeV calculated within the UrQMD model.

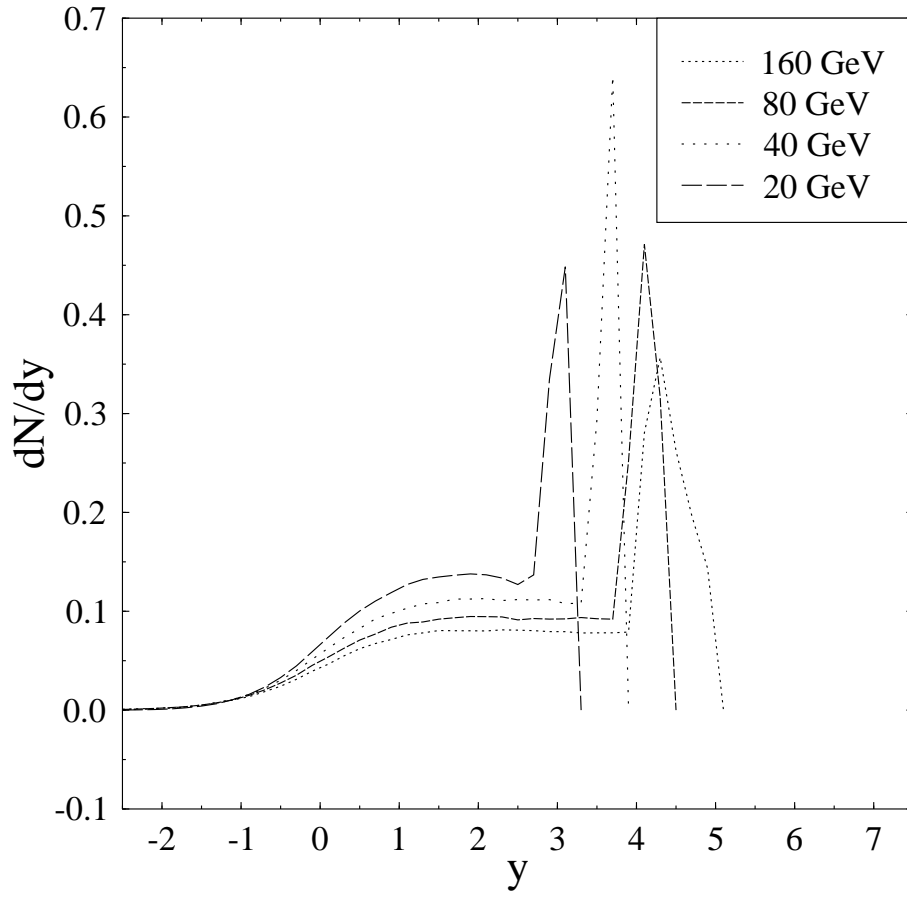


Figure 4.3: The rapidity distribution of \bar{p} in $\bar{p}+p$ collisions at $\sqrt{s} = 20, 40, 80$ and 160 GeV calculated within the UrQMD model.

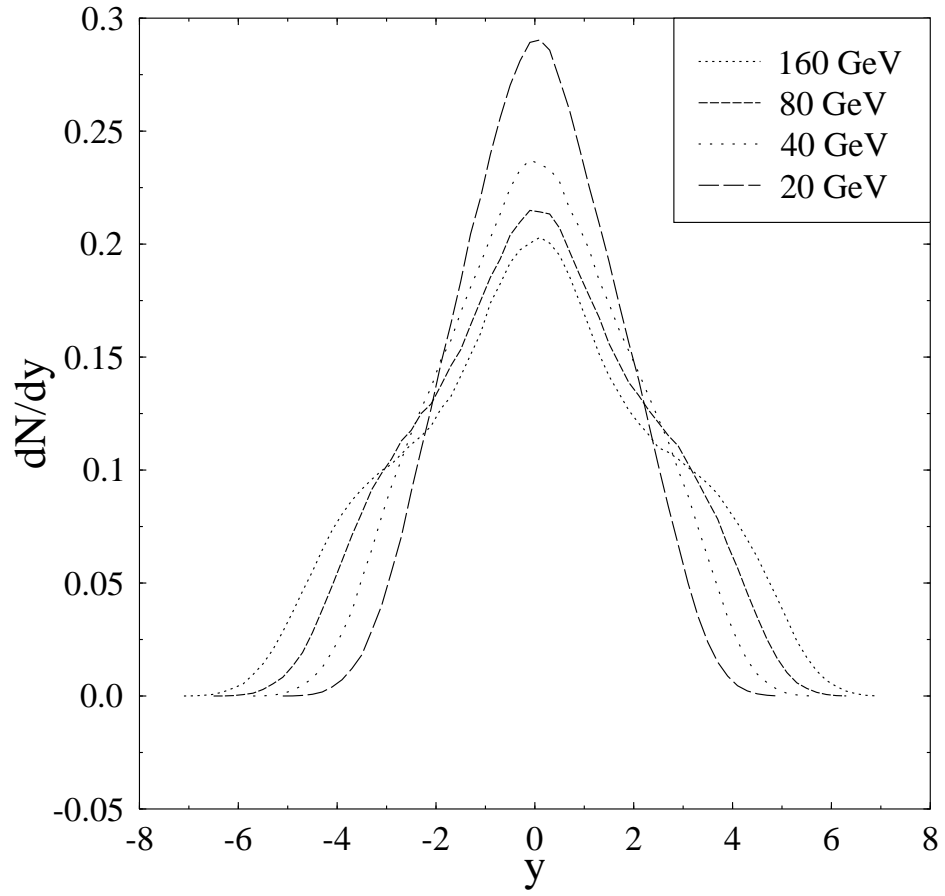


Figure 4.4: The rapidity distribution of π^0 in $\bar{p} + p$ collisions at $\sqrt{s} = 20, 40, 80$ and 160 GeV calculated within the UrQMD model.

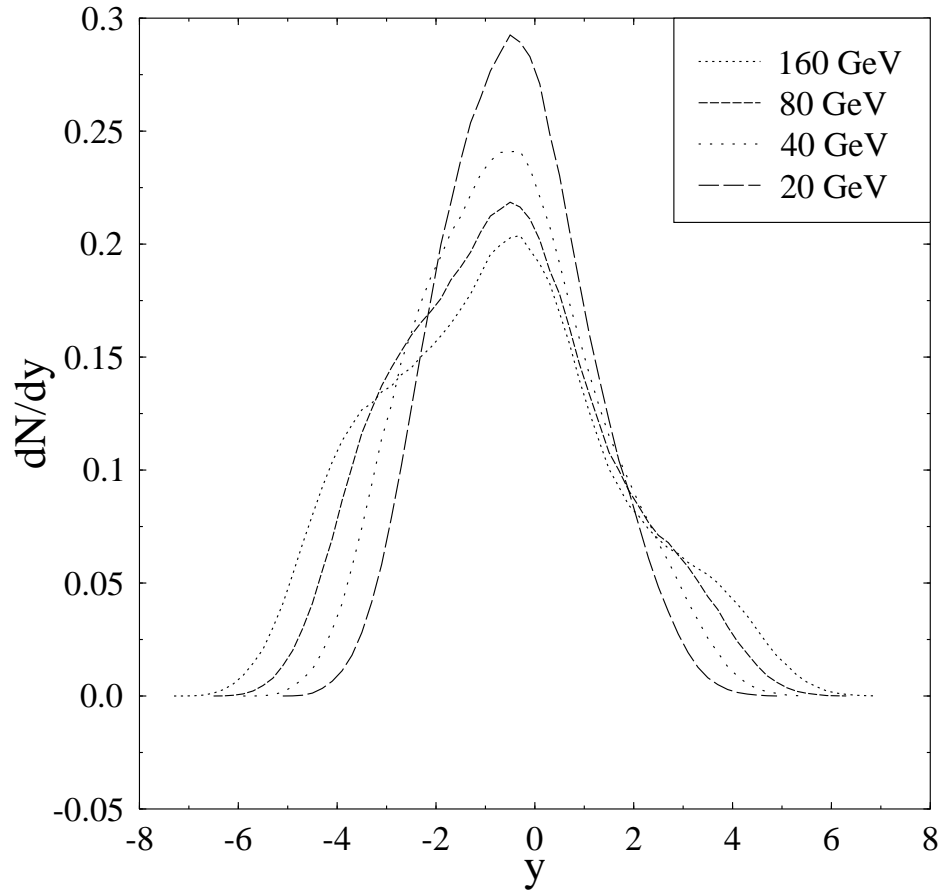


Figure 4.5: The rapidity distribution of π^+ in $\bar{p} + p$ collisions at $\sqrt{s} = 20, 40, 80$ and 160 GeV calculated within the UrQMD model.

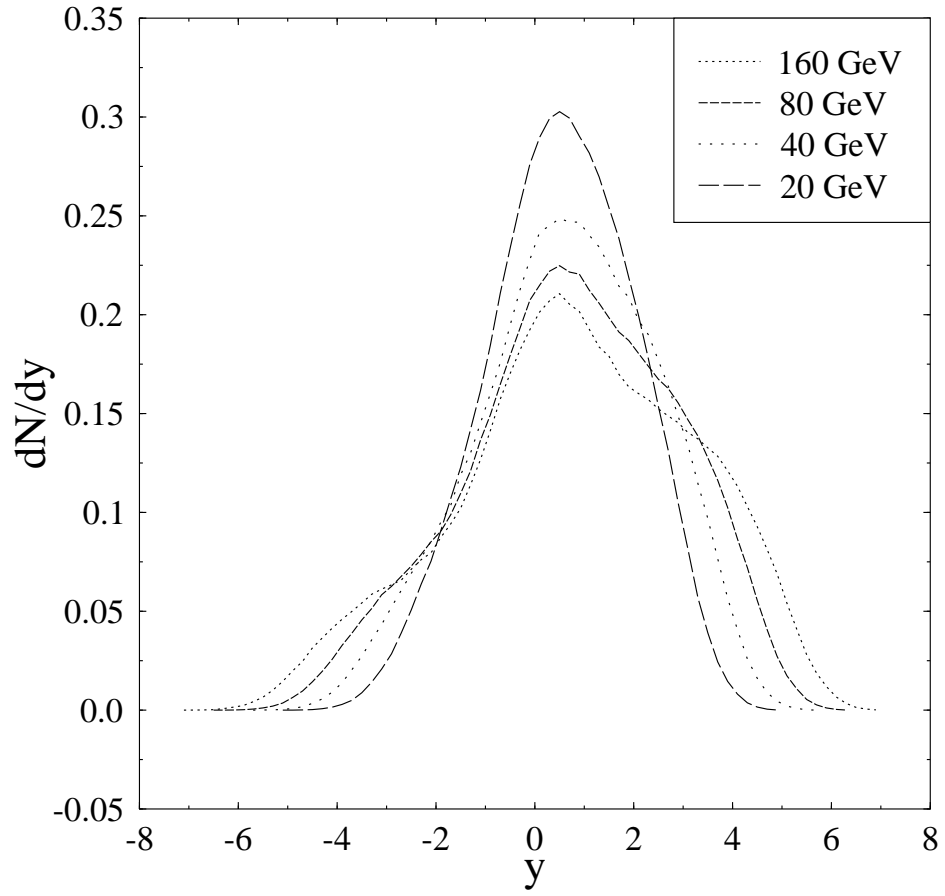


Figure 4.6: The rapidity distribution of π^- in $\bar{p} + p$ collisions at $\sqrt{s} = 20, 40, 80$ and 160 GeV calculated within the UrQMD model.

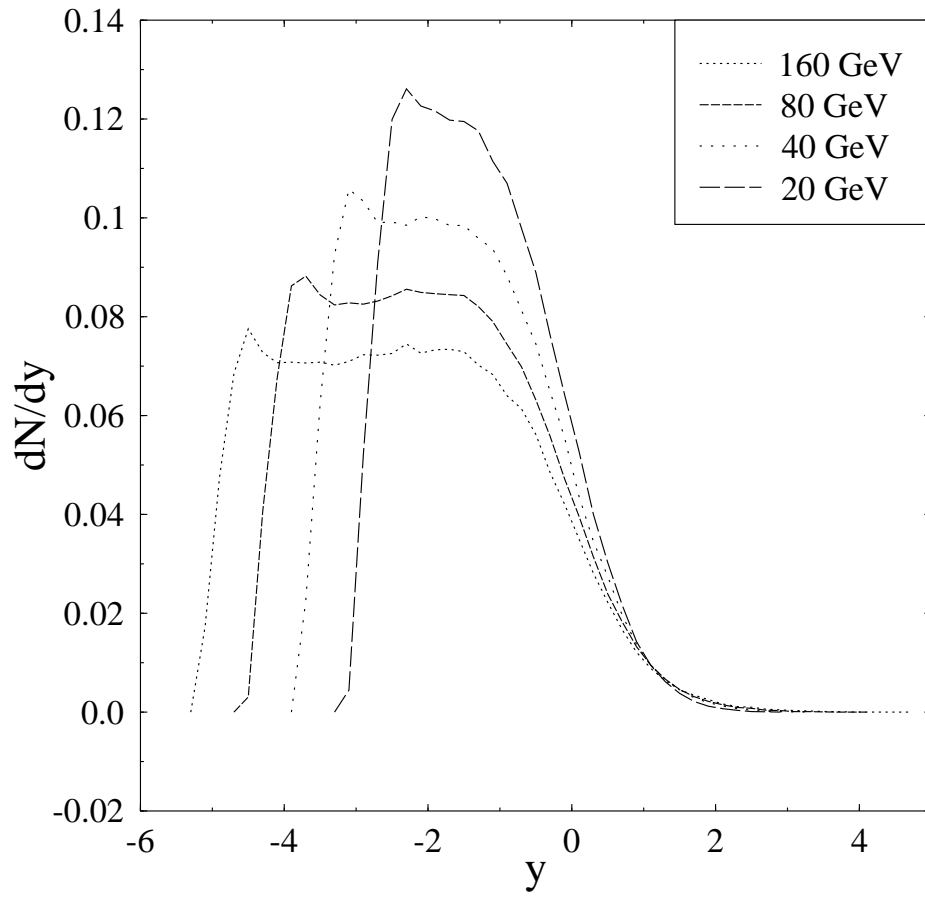


Figure 4.7: The rapidity distribution of n in $\bar{p} + p$ collisions at $\sqrt{s} = 20, 40, 80$ and 160 GeV calculated within the UrQMD model.

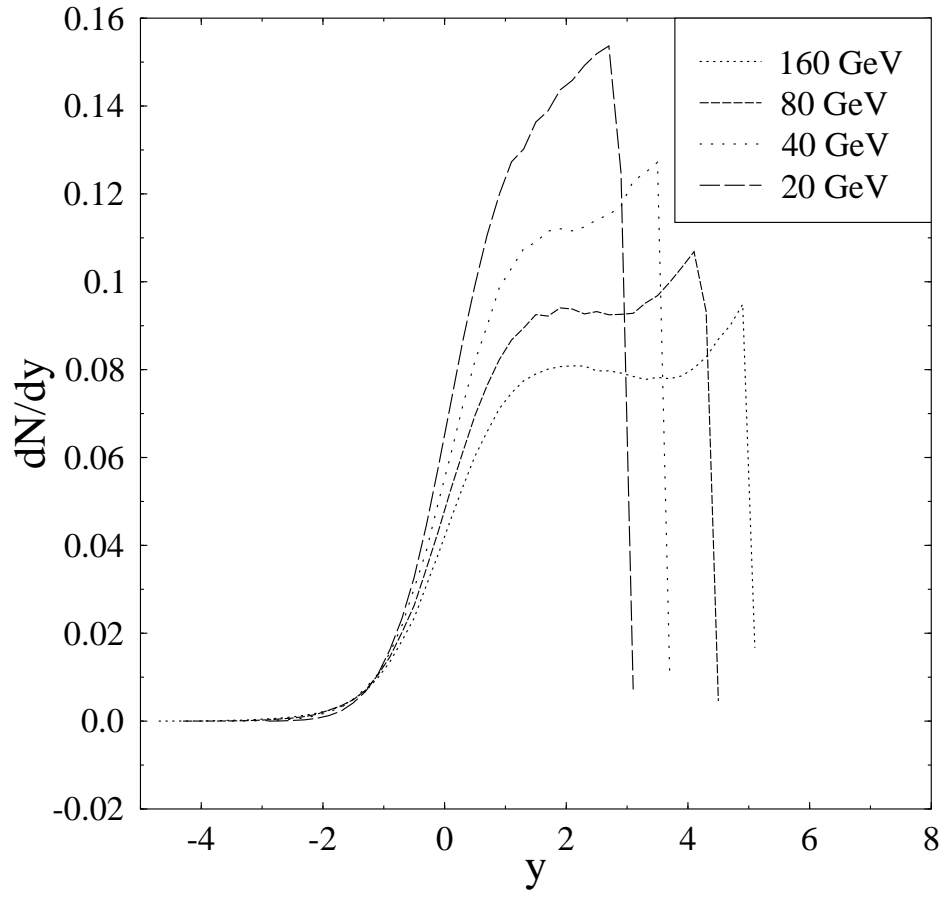


Figure 4.8: The rapidity distribution of \bar{n} in $\bar{p} + p$ collisions at $\sqrt{s} = 20, 40, 80$ and 160 GeV calculated within the UrQMD model.

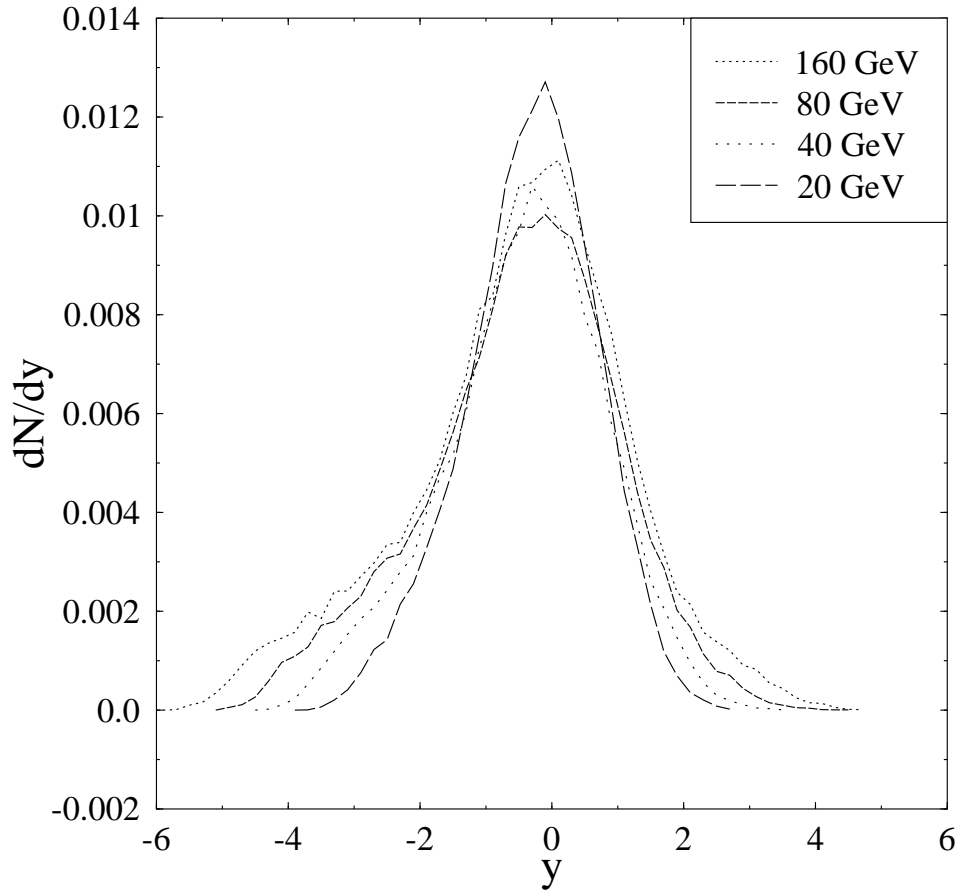


Figure 4.9: The rapidity distribution of K^+ in $\bar{p} + p$ collisions at $\sqrt{s} = 20, 40, 80$ and 160 GeV calculated within the UrQMD model.

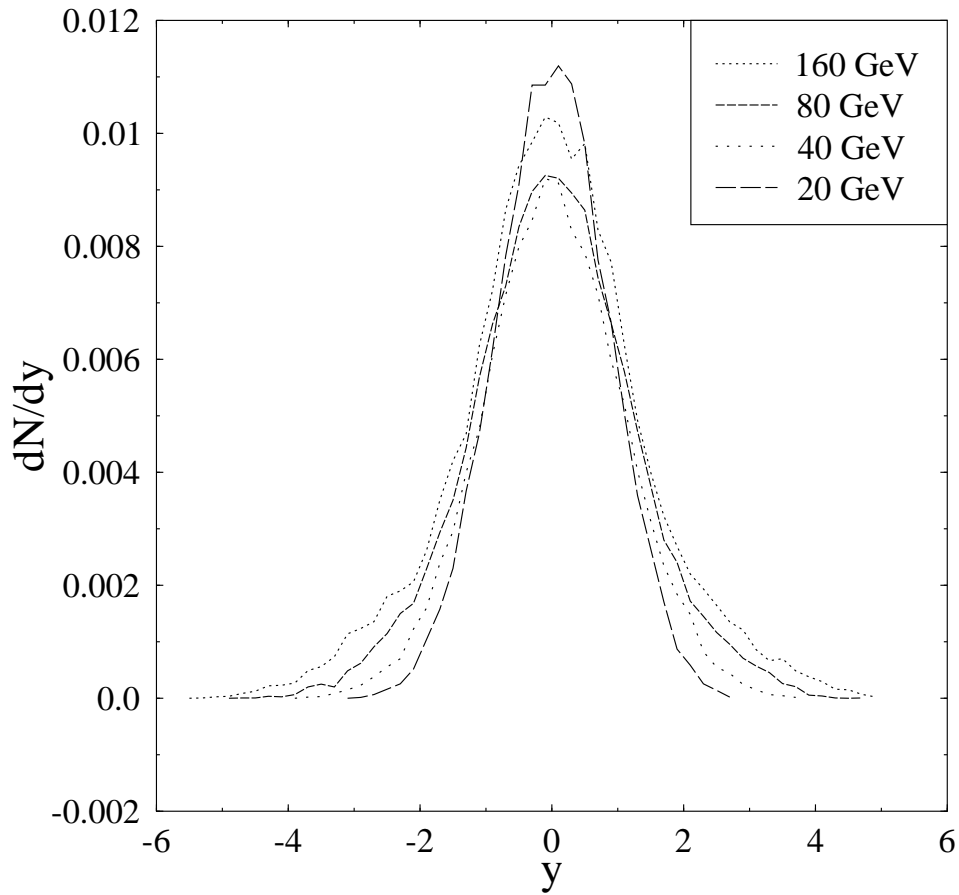


Figure 4.10: The rapidity distribution of K^- in $\bar{p} + p$ collisions at $\sqrt{s} = 20, 40, 80$ and 160 GeV calculated within the UrQMD model.

The rapidity distributions of K^+, K^-, K^0 and \bar{K}^0 are presented in Figs. (4.9), (4.10), (4.11) and (4.12), respectively. Unlike the π^0 distribution, Fig.(4.11) and Fig.(4.12) show that the rapidity distributions of K^0 and \bar{K}^0 are not symmetric although both K^0 and \bar{K}^0 are neutral particles. It is found that $K^0(d\bar{s})$ and $\bar{K}^0(\bar{d}s)$ are produced a bit more in the p and \bar{p} directions, respectively. The

distributions of K^0 and \bar{K}^0 are very interesting results which may tell us some important dynamics. Further studies need to be carried out to draw concrete conclusions.

We may tentatively understand the distributions of K^0 and \bar{K}^0 by considering the different masses of the d and s quarks. It is believed that the s quark is heavier than the u and d quarks. In the constituent quark models, we usually set the mass of u and d quarks about $0.36 \text{ GeV}/c^2$ and the mass of the s quark about $0.54 \text{ GeV}/c^2$ while the so-called current quarks masses are $m_u = 1.5$ to 5 MeV , $m_d = 3$ to 9 MeV , and $m_s = 60$ to 170 MeV for the u , d and s quarks, respectively. One may expect that more s and \bar{s} quarks are created in the directions of \bar{p} and p , respectively, hence more $\bar{K}^0(\bar{d}s)$ and $K^0(d\bar{s})$ are respectively produced in the directions of \bar{p} and p .

4.3 Transverse mass distribution

The transverse mass distributions for N , \bar{N} , π and K particles are presented in Fig.(4.13) to Fig. (4.15). It is found:

- (1) more particles are produced in the transverse direction at lower center-of-mass energies;
- (2) particles are mainly created with small transverse momenta;
- (3) π are the dominant particles produced in the transverse direction which confirm the fact that p and \bar{p} are dominantly from the elastic collision while n and \bar{n} are mainly created in the charge exchange process.

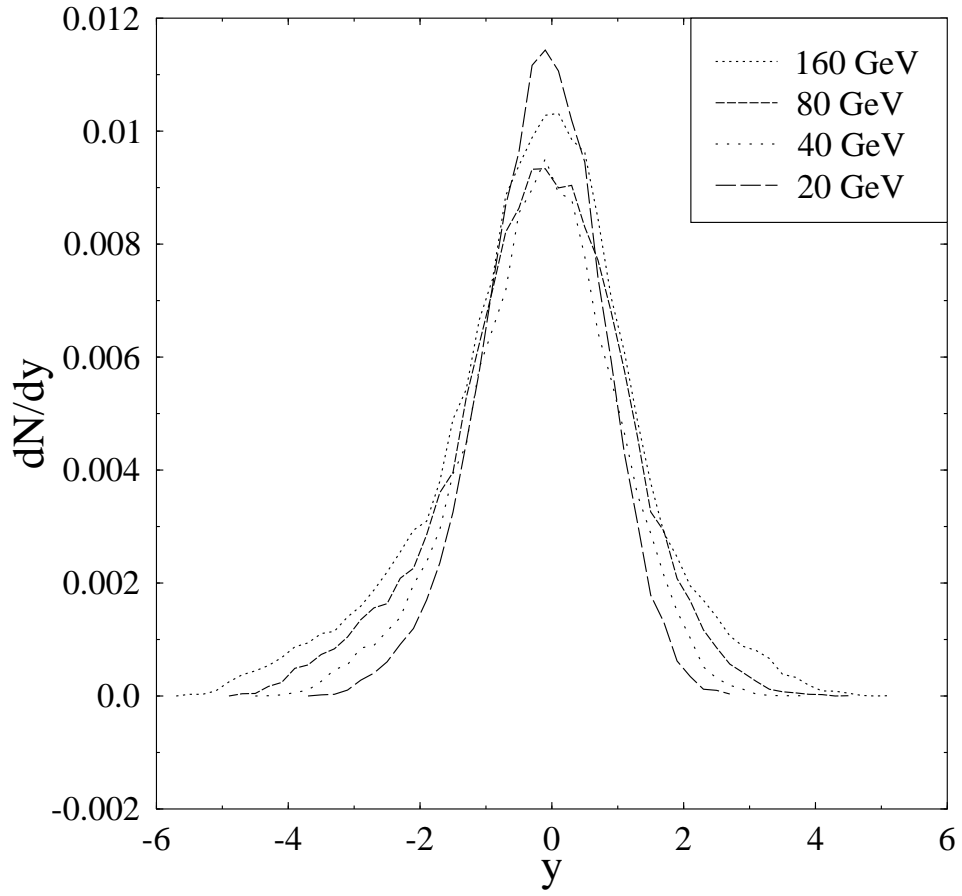


Figure 4.11: The rapidity distribution of K^0 in $\bar{p} + p$ collisions at $\sqrt{s} = 20, 40, 80$ and 160 GeV calculated within the UrQMD model.

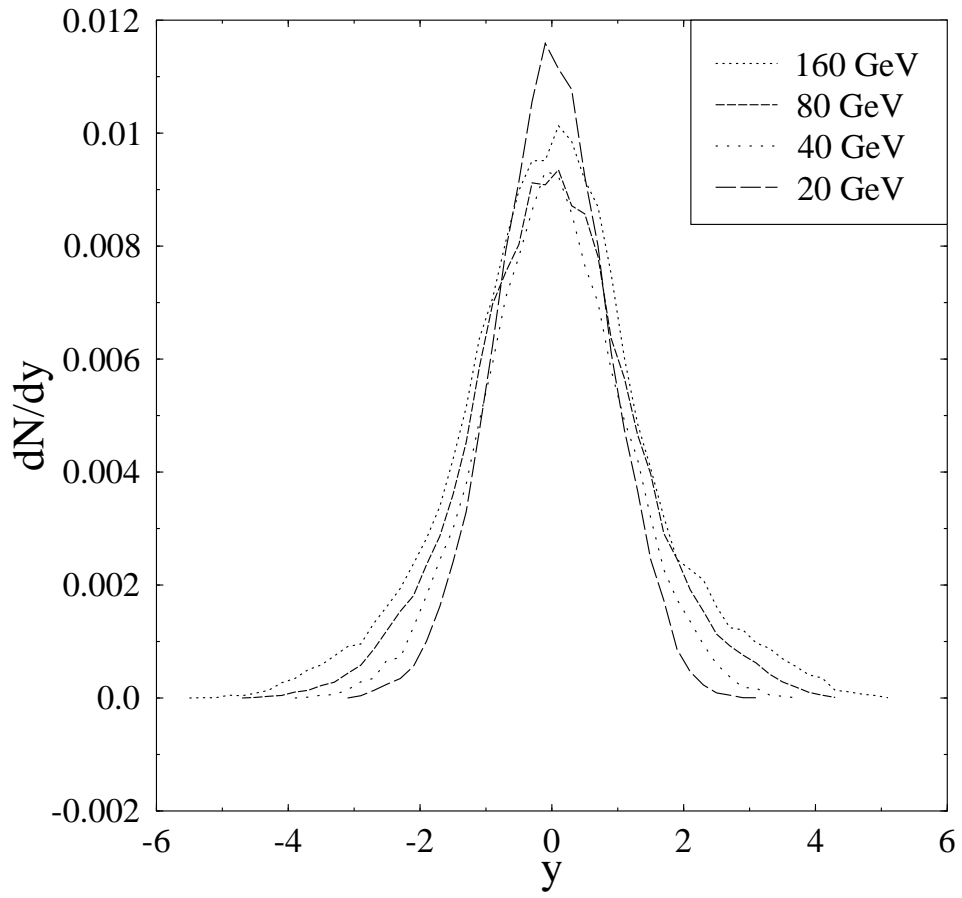


Figure 4.12: The rapidity distribution of \bar{K}^0 in $\bar{p} + p$ collisions at $\sqrt{s} = 20, 40, 80$ and 160 GeV calculated within the UrQMD model.

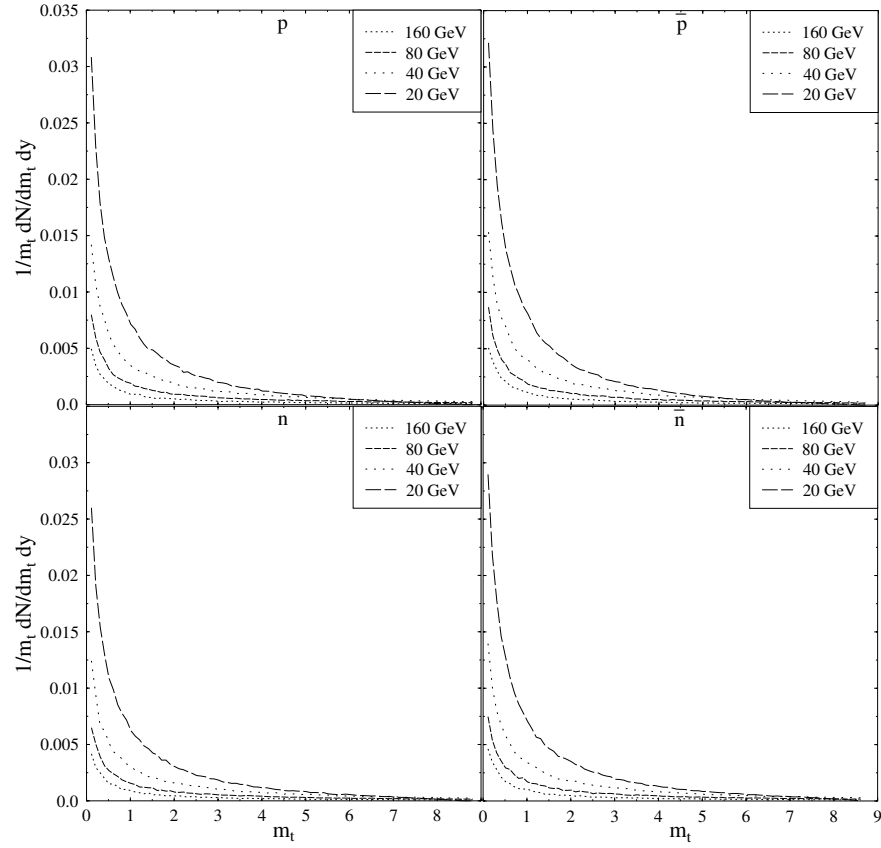


Figure 4.13: Transverse mass distribution of p, \bar{p}, n, \bar{n} in $\bar{p} + p$ collisions at $\sqrt{s} = 20, 40, 80$ and 160 GeV calculated within the UrQMD model.

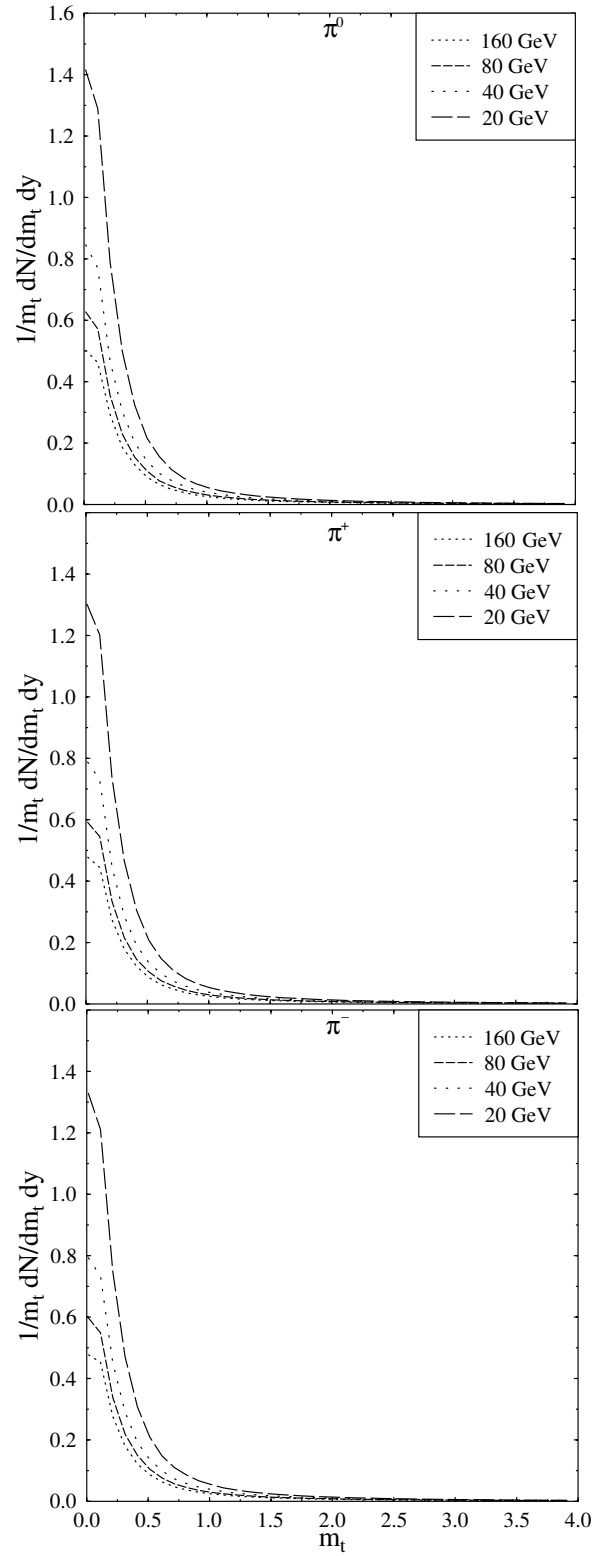


Figure 4.14: Transverse mass distribution of π^0, π^+, π^- in $\bar{p} + p$ collisions at $\sqrt{s} = 20, 40, 80$ and 160 GeV calculated within the UrQMD model.

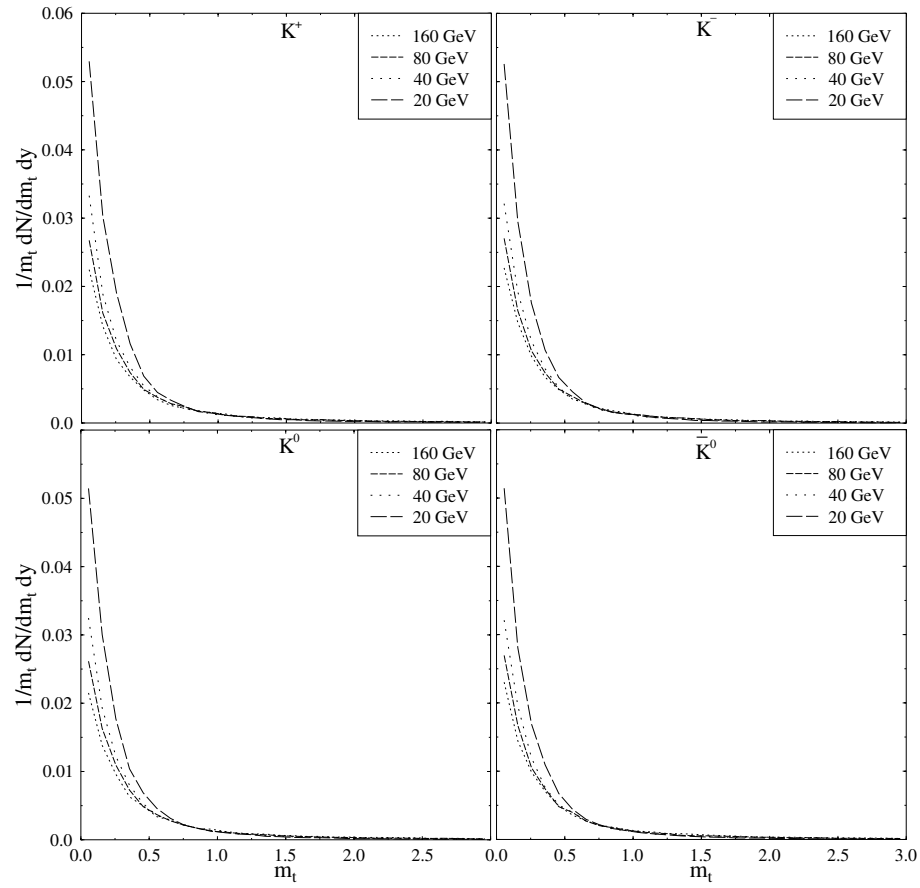


Figure 4.15: Transverse mass distribution of K^+ , K^- , K^0 , \bar{K}^0 in $\bar{p} + p$ collisions at $\sqrt{s} = 20, 40, 80$ and 160 GeV calculated within the UrQMD model.

4.4 Summary

In this work we have preliminarily studied the $\bar{p}p$ interactions at $\sqrt{s} = 20, 40, 80$ and 160 GeV using the UrQMD model. The particle yields and rapidity and transverse mass distributions are worked out for the particles $\pi^0, \pi^+, \pi^-, K^0, \bar{K}^0, K^+, K^-, p, \bar{p}, n$, and \bar{n} . From this preliminary investigation, one may extract some points:

1. the total yields for all particles increases slightly with the center-of-mass energies ranging from 20 to 160 GeV;
2. the energy-dependence of the yield for a certain particle is very light in the energy region considered;
3. positively-charged particles are likely to be produced in the p direction while negatively-charged particles are likely to be produced in the \bar{p} direction;
4. more particles with higher energies are produced at higher incoming energies.
5. that the s quark is heavier than u, d quarks might be indicated in the Kaons production.

REFERENCES

REFERENCES

- Abachi, S. et al. (1995). Search for High Mass Top Quark Production in $p\bar{p}$ Collisions at $\sqrt{s}=1.8$ TeV. **Physical Review Letter** 74: 2422-2426.
- Abachi, S., Abbott, B. et al. (1995). Observation of the Top Quark. **Physical Review Letter** 74: 2632-2637.
- Abachi, S., Abbott, B., Abolins, M. et al. (1995). Inclusive μ and b-Quark Production Cross Sections in $p\bar{p}$ Collisions at $\sqrt{s}=1.8$ TeV. **Physical Review Letter** 74: 3548-3552.
- Abachi, S., Abbott, B., Abolins, M., Acharya, B. S. et al. (1996). Isolated Photon Cross Section in the Central and Forward Rapidity Regions in $p\bar{p}$ Collisions at $\sqrt{s}=1.8$ TeV. **Physical Review Letter** 77: 5011-5015.
- Abe, F. et al. (1998). Measurement of the Differential Cross Section for Events with Large Total Transverse Energy in $p\bar{p}$ Collisions at $\sqrt{s} = 1.8$ TeV. **Physical Review Letter** 80: 3461-3466.
- Ackermann, K.H. et al. (1999). The STAR Time Projection Chamber. **Nuclear Physics A** 661: 681c-685c.
- Afanasiev, S.V. et al. (1999). The NA49 large acceptance hadron detector. **Nuclear Instruments and Methods in Physics Research Section A** 430: 210-244.
- Afanasiev, S.V., Anticic, T. et al. (2002). Energy dependence of pion and kaon production in central Pb+Pb collisions. **Physical Review C** 66: 054902.

- Aichelin, J. (1991). Quantum Molecular Dynamics- A Dynamical Microscopic n-body approach to investigate fragment formation and The Nuclear Equation of State in Heavy Ion Collisions. **Physics Report** 202: 233-360.
- Aichelin, J., Peilert, G., Bohnet, A., Rosenhauer, A., Stoecker, H. and Griner, W. (1998). Quantum molecular dynamics approach to heavy ion collisions: Description of the model, comparison with fragmentation data, and the mechanism of fragment formation. **Physical Review C** 37: 2451-2468.
- Arnison, G. et al. (1983). Experimental observation of isolated large transverse energy electrons with associated missing energy at $\sqrt{s}=540$ GeV. **Physics Letter B** 122: 103-116.
- Barannikova, O. and Wang, F. (2003). Mid-rapidity π^\pm , K^\pm , \bar{p} spectra and particle ratios from STAR. **Nuclear Physics A** 715: 458c-461c.
- Barnett, R. M. et al. (1996). Review of Particle Physics. **Physical Review D** 54: 1-708.
- Bass, S. A., Belkacem, M., Bleicher, M. et al. (1998). Microscopic Models for Ultrarelativistic Heavy Ion Collisions. **Progress in Particle and Nuclear Physics** 41: 225-370.
- Bleicher, M. et al. (1999). Relativistic Hadron-Hadron Collisions in the Ultra-Relativistic Quantum Molecular Dynamics Model. **Journal of Physics G** 25: 1859-1896.
- Bodmer, A. R. and Panos, C. N. (1977). Classical microscopic calculations of high-energy collisions of heavy ions. **Physical Review C** 15: 1342-1358.

- Bonche, P., Koonin, S. and Negele, J. W. (1976). One-dimensional nuclear dynamics in the time-dependent Hartree-Fock approximation. **Physical Review C** 13: 1226-1258.
- Bratkovskaya, E. L., Bleicher, M., Reiter, M., Soff, S., Stoecker, H., Leeuwen, M., Bass, S. A. and Cassing, W. (2004). Strangeness dynamics and transverse pressure in relativistic nucleus-nucleus collisions. **Physical Review C** 69: 054907.
- Broniowski, W. and Florkowski, W. (2002). Geometric relation between centrality and the impact parameter in relativistic heavy-ion collisions. **Physical Review C** 65: 024905.
- Kraus, I. (2004). System size dependence of strangeness production at 158 AGeV. **Journal of Physics G** 30: S583-S588.
- Kruse, H., Jacak, B. V., Molitoris, J. J., Westfall, G. D. and Stoecker, H. (1985). Vlasov-Uehling-Uhlenbeck theory of medium energy heavy ion reactions: Role of mean field dynamics and two body collisions. **Physical Review C** 31: 1770-1774.
- Mischke, A. et al. (2002). Lambda production in central $Pb + Pb$ collisions at CERN-SPS energies. **Journal of Physics G** 28: 1761-1768.
- Mohl, D., Petrucci, G., Thorndahl, L. and van der Meer, S. (1980). Physics and technique of stochastic cooling. **Physics Report** 58: 73-102.
- Muhm, A., Gutsche, T., Thierauf, R., Yan, Y. and Faessler, A. (1996). $p\bar{p}$ annihilation into two mesons in the quark annihilation model including final state interaction. **Nuclear Physics A** 598: 285-317.

Uhling E. A. and Uhlenbeck, G. E. (1933). Transport Phenomena in Einstein-Bose and Fermi-Dirac Gases. **Physical Review** 43: 552-561.

Weber, H., Bratkovskaya, E. L. and Stoecker, H. (2002). Nucleus-nucleus collisions at high baryon densities. **Physics Letter B** 545: 285-290.

Zabrodin, E. E. et al. (1995). Inclusive spectra of charged particles in pp and $\bar{p}p$ interactions at 32 GeV/c. **Physical Review D** 52: 1316-1342.

CURRICULUM VITAE

NAME: Mr. Ayut Limphirat

DATE OF BIRTH: May 10, 1981

PLACE OF BIRTH: Ratchaburi Province, Thailand

NATIONALITY: Thai

E-MAIL: limphirat@yahoo.com, ayut@physics2.sut.ac.th

EDUCATIONS:

Master of Science (2002 - 2004)

School of Physics, Suranaree University of Technology, Thailand

Field of Study: Nuclear and Particle Physics

Title of Thesis: Simulation of $\bar{p}p$ interactions using UrQMD model

Supervisors: Dr. Chinorat Kobdaj and Assoc. Prof. Dr. Yupeng Yan

Bachelor of Science (1998 - 2001)

Department of Physics, Chulalongkorn University, Bangkok, Thailand

Field of Study: Material Science

Title of Thesis: Hardening of 96.5 percent Gold by Microalloying

Supervisor: Assoc. Prof. Dr. Phatana Phavanantha